Study on biological transport network utilizing plasmodium of *Physarum polycephalum* (モジホコリ変形体を用いた生物学的輸送ネットワークの研究)

AKITA Dai (秋田 大)
Graduate School of Life Science, Hokkaido University

March, 2017

Contents

Abstract

Vein networks found in various organisms such as leaf veins, bronchial tree, and blood vessels have a crucial role to transport substances fast and efficiently, so that it is expected to provide physical significance on morphology by revealing relationship between geometrical structure of transport network and transport ability. However, most biological transport networks have difficulties on culture methods in experimental environment, discouraging repetitive experiment. Moreover, design of transport network is a multi-objective problem such as total volume cost of network and coverage of region, which make it harder to evaluate trasport ability.

Meanwhile, a true slime mold, *Physarum polycephalum*, attracts attention recently as a model organism of biological transport network. In a stage of its life-cycle called plasmodium, it forms a giant multi-nuclear single amoeboid cell, creating tubular structure for flow of prosoplasms. This tubular network also has an important role of locomotion and distribution of nutrients, and therefore, if plasmodium touches some food sources, vein network connecting them emerges overnight. Some researches exploit this behavior to solve geometrical problems such as maze and design of railway network and analyzed mainly the connectivity of network, whilst the view point of transport has been rarely discussed ever.

For the purpose of evaluation of transport ability, we developed an experiment utilizing *Physarum polycephalum* and analyzed the results. In the experiment, a uniform plasmodium without vein structure was put on a confined space created on agar, which had one narrow exit to a food source. Thus, as the plasmodium moves through the exit, a vein network to transport body mass emerges and develops with the evacuation from the arena. This experiment enables us to observe emergence of transport network and draining process from a two-dimensional area to one point by the network.

As an analysis of transportation by the emerged network, we estimated plasmodial thickness and its decreasing speed at each point of the confined space from the time-lapse images. The result showed that the plasmodium was drained with the same time course despite the distance from the exit, except for the points of main veins. Moreover, this property was confirmed for different shapes of arena, which implied shape-adaptive ability of plasmodium to construct transport networks causing homogeneous draining.

To investigate what factors originate in this homogeneous draining, we analyzed coverage rate of network to arena, suggesting to use Hausdorff distance as an index of coverage. Hausdorff distance between a network and an arena means, in brief, the least distance by which any point in the arena can reach a point of the network. Therefore, lower Hausdorff distance implies higher coverage, and vice versa. The calculation for plasmodial network showed Hausdorff distance of 10% to 20% of diameter of the arena. This higher coverage of networks may be a factor of the homogeneous draining.

Furthermore, we tried fluid dynamical approach under the assumption of Hagen-Poiseuille flow, according to which flow rate and applied pressure of a tube consisted proportional relationship of which coefficient, called conductivity, was determined by the length and the radius. Under this assumption, we calculated hydrodynamical conductivity from each point of the network to the exit. Then the contour line of conductivity expanded similarly to the shape of arena, that is, the hydrodynamic accesibility is not developed with eucridian distance, which supports the mass draining independent of distance.

In addition to these analysis, we validated a well-known rule of transport network, Murray's law, which was stated by Murray in 1926. According to the law, when a artery with radius r_0 ramifies into arteries with radii r_1 and r_2, they have relationship $r_0^3 = r_1^3 + r_2^3$. Because Murray derived this relationship by considering minimization of frictional loss of flow and volume cost, establishment of the law implies optimization of them. Therefore, we estimated the exponent of the relationship for plasmodial network in the experiment, and 95% confidence interval $[2.53, 3.29]$ was obtained. This result supports Murray's law on vein network of *Physarum polycephalum* and implies optimization of trade-off between frictional energy loss and total volume cost.

To investigate the mathematical background of these network formation, we applied a model called current-reinforcement to simulate the experimental environment. In the model, slime mold is expressed as a random mesh network, and quantity D of each edge, which corresponds to diameter of edge, develops according to a formula $dD/dt = Q^\mu - D$, where Q and μ are flow rate and a positive parameter, respectively. In other words, a vein with larger flow is thickened, and with lesser flow is thinned. Here, because it needs information of sources and sinks to find flow rate of each edge, we set every node except for the exit as a source of the same quantity and the exit as the only one sink. With these settings, the simulation converged to a steady state, in which tree structure without loop is obtained for $\mu > 1$, and relatively uniform vein structure with loops for $\mu \leq 1$.

In the similar manner to the analysis of experimental data, the Hausdorff distance was calculated for the simulated networks. The result shows that networks with $\mu > 1$ gave similar values to the experimental ones, while $\mu \leq 1$ had worse coverage. Especially, networks of $\mu = 4/3$ are found to be optimized according to evaluation of friction energy and total volume. In fact, the parameter $\mu = 4/3$ is closely bounded with Murray's law which was derived from optimization of friction energy and total volume cost. Assuming a steady state of current-reinforcement, we can derive proportional relationship between Q and $r^{4/\mu}$, so that $\mu = 4/3$ corresponds to Murray's law. Hence, the experimental validation of Murray's law means suitability of $\mu = 4/3$ as a parameter of current-reinforcement. This apparent parameter correspondence has not been discussed on studies of current-reinforcement model and is, therefore, new discovery on plasmodial network. Moreover, the revealed relationship between models of blood vessels and slime mold is important result showing usefulness of slime mold as a model organism of morphological study.

Chapter 1

Introduction

Biological transport networks form part of the critical infrastructure that is required to distribute resources and information rapidly and efficiently throughout the entire body of a multicellular organism. They include the vascular systems of plants, animals, gastrovascular system of hydractiniid hydroids that are embedded within the organism, the plasmodial veins of slime molds, and the mycelial cords of fungi that effectively constitute the entire organism apart from the reproductive structures. These networks play a key role in the organization of the overall body plan, and the vessel size and network architecture are thought to follow quarter-power allometric scaling laws that relate the notional space-filling fractal branching pattern of the network to body size and metabolic rate according to metabolic scaling theory (MST) [1], or reflect the design of optimal transport networks [2–4].

In each case, the network comprises tubular elements with varying thickness and length, that are organised as a hierarchical branching tree, but may also contain a significant number of additional loops to improve performance under fluctuating loads or in the presence of damage [5, 6]. Whilst the vessel geometry clearly has an impact on the local fluid flow, the overall transport behaviour and scaling relationships are properties of the entire network. Unfortunately, however, most biological networks develop over extended time periods, cannot be characterised easily in their entirety, and are not amenable to manipulation or repetition, making it difficult to experimentally evaluate competing theories of network organisation and scaling exponents against empirical data.

Recently, attention has focussed on the true slime mold, *Physarum polycephalum*, as a tractable model organism to study the iterative interplay between structure and function in a self-organised biological transport network, and to help to determine the rules that may govern adaptive network development [7–15]. *Physarum polycephalum* is a giant, single-celled amoeboid organism that grows rapidly as an extensive plasmodial network over the available space within a few hours as it forages for food. If resources are not located, it can also retract the plasmodium and redeploy the biomass elsewhere to support further foraging.

Here we exploit this latter behaviour to examine network formation during evacuation of the plasmodium from a set of arenas with varying geometric shape. Within a few hours, an intricate network develops within the initially uniform plasmodial sheet, that then serves to progressively transport biomass out of the arena via the single exit point. As the entire system is accessible, we can determine quantitatively: (i) the dimensions of

the individual veins; (ii) the structure of the network that they form, including the space filling properties; (iii) how these contribute to the rate of biomass retrieval over the entire arena; (iv) whether the network that forms follows predicted scaling relationships at the vein junctions; and (v) how these parameters vary as the network adapts to different arena geometry. Based on these properties, we discuss adaptivity of the network formation for different shapes of arena and function of biological transport network, suggesting a new view point of biological information processing on information hub.

In particular, we have examined whether the branching rule, originally proposed by Murray to describe the branching of arteries [16], holds for vein networks in *Physarum*. Murray proposed that the relationship:

$$r_0^3 = r_1^3 + r_2^3, \tag{1.1}$$

where r_0 is the radius of parent vein and r_1 and r_2 are those of daughter veins, provides an optimal solution to balance the effect of reducing viscous drag with the cost of increasing vessel volume, assuming Hagen-Poiseuille flow. Murray's law has been validated by measurements of artery branching relationships for small vessels, that typically give an exponent ranging from 2.7 to 3.0 [17], and is often incorporated in predictions of network performance as a transition between area-preserving (r^2) for branching in large vessels to r^3 for branches closer to the terminal transport vessels (e.g., [1,4]). Nevertheless, many of the assumptions underpinning these universal theories lack strong experimental support and are the subject of ongoing debate (e.g., [18]). Indeed, recent automated non-invasive measurements of vessel properties in vascular networks have been used to explicitly test different predictions for the scaling exponents from several theoretical models, concluding that none of the current methods provides a good description of real vascular networks, and they advocated the development of new relationships between vessel geometry and global network properties [19]. It is therefore important to link experimental measurements of vessel properties, with theoretical principles, such as Murray's Law, that govern idealised network behaviour, when constructing predictive models of network organisation and performance in *Physarum*.

For the purpose of pursuing the mechanisms of amoeboid movement, peristatic waves and network formation in pllasmodium of *Physarum polycephalum*, a number of bioinspired mathematical models have already suggested [8,14,15,20–26]. In the case of network formation, current-reinforcement models [7, 8, 14] capture the behaviour of the biological system well, but so far none have been explicitly parametised from experimental results. Current reinforcement models include a non-linear current-reinforcement term that reflects the propensity of a tube to increase in diameter in response to the internal flow rate through the tube itself. Conversely, if the flow is too small the tube disappears at a rate determined by the decay term. By following the time-evolution of evacuation network formation, we can begin to link the experimental observations with appropriate values for the coefficients in the model.

We applied this model to simulate the experimental environment and emergence of tubular network, with various parameters of current-reinforcement term. Here, we have made simplifying assumptions, most notably that the time-scale for network formation (hours) allows us to neglect the complex viscoelastic properties of the plasmodial body and contraction-relaxation based shuttle streaming (min). Instead, we treat the plasmodial

veins as rigid cylindrical pipes in each time step, but with the capacity to change average radius in response to fluid flow in the next time step. Thus, correspondence of current-reinforcement parameter to real vein network and factor of vein development are discussed by combining results of the experiment and simulation.

Chapter 2

Backgrounds and Reviews

2.1 Rules of transport network

In this paper, we let *transport networks* denote a variety of network structures with a function to transport substances, resources, informations and so on, which range from winding and branching rivers to biological vein networks like blood vessels and leaf veins, of course including kinds of urban infrastructures such as road or train networks. Hence, transport networks are ubiquitous in the world and have attracted researchers of various regions, some of which eventually found rules on them.

2.1.1 Horton's law on river network

River, obviously, transports water from higher mountains to sea or lake through winding streams repeating merging and branching, and the first mordern insight was given by James Hatton, who was educated as a physician but interested in geology. Establishing an earlier concept of uniformitarianism, he formulated his own theory of geology, which was published as an article of the transactions of the royal society of Edinburgh [27] in 1788 and as a two-volume book [28] in 1795. However, these publications attracted less attention and rather strong criticism [29]. After Hutton's death, John Playfair, a professor of mathematics, wrote a book summarizing clearly Hutton's theory with persuasive comments, which was, on the contrary, so widely read that geological thinking was heavily affected [29, 30].

Robert Elmer Horton, a hydrologist of twentieth century, was one of researchers impressed by Playfair's book, so that he cited from it the following famous statement so-called *Playfair's law* in his work of 1945 [31]:

> "Every river appears to consist of a main trunk, fed from a variety of branches, each running in a valley proportioned to its size, and all of them together forming a system of vallies, communicating with one another, and having such a nice adjustment of their declivities that none of them join the principal valley either on too high or too low a level."

However, discussions on physiography at that time had still remained qualitative, motivating him to study river system quantitatively.

He suggested an original stream ordering system [31] and considered relationships be-

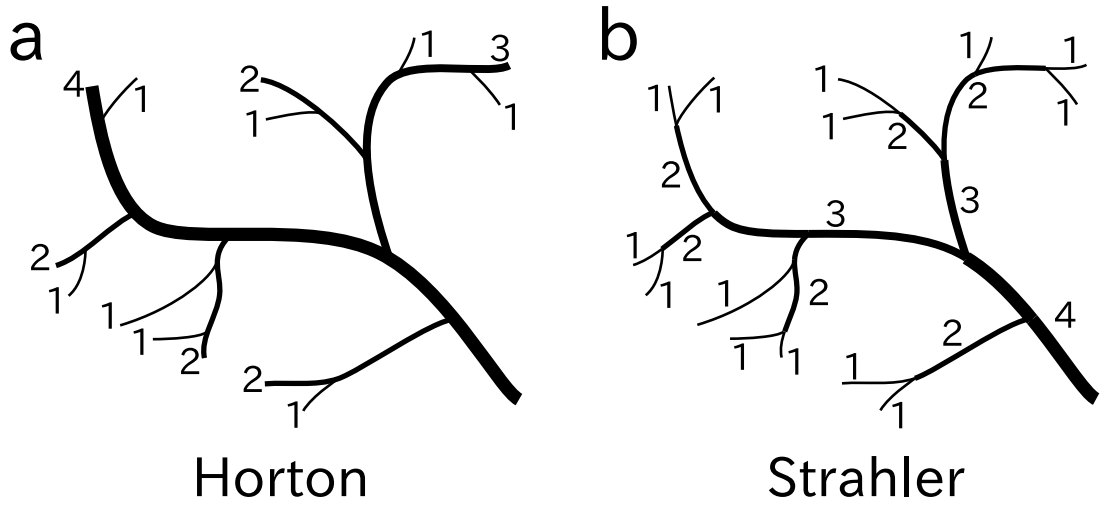

Fig. 2.1 Example of river ordering system of Horton (a) and Strahler (b).

tween orders and branch numbers, stream length, or basin area. According his rules of the ordering system, orders of streams are given as follows:

1. Assign 1 for streams having no tributary.
2. When streams having different orders join, order of the parent stream is set to the greatest order of the tributaries, except for the case streams have the same order ω, in which instead the parent stream is given order $\omega + 1$.
3. When streams having the same order ω join, the parent stream is given order $\omega + 1$. At the same time, the main stream is selected from the tributaries as the stream joining the parent stream at the smallest angle, but exceptional selection is allowed. The order of the main stream is reset to the same with the parent stream up to the source.

As an example is shown in Fig. 2.1a, lower order streams appears frequently and have lower length, in contrast to the lesser number and longer length of higher order streams. In fact, Horton found that the number N_ω of streams having order ω decreased exponentially, that is, there existed a *bifurcation ratio* R_b for which

$$N_\omega = R_b^{\Omega-\omega}, \tag{2.1}$$

where Ω is the maximum order of the river system. Similarly, given that l_ω denotes the average length of streams having order ω, there exists a *length ratio* R_l such that

$$l_\omega = l_1 R_l^{\omega-1}. \tag{2.2}$$

Moreover, such exponential relationship holds for slope and area of basin. This series of laws of stream order is called *Horton's law*, verified by other morphometric analyses [32,33].

After Horton's work, many other ordering rules were proposed [34, 35]. Among them, the ordering system revised from Horton's one by Arthur Newell Strahler [36] has been accepted widely. His ordering rule abolished the third rule written above, obviating determination and reordering of the main stream (Fig. 2.1b). Despite this modification,

Horton's law still hold [36], and some researchers used Strahler's method instead of Horton's [37–39]. Especially, Strahler's ordering system has a topological characteristics, that is, orders of streams of a river network are determined by its topological nature of connections.

Strahler's ordering system has, in addition to the simpler rules, a topological characteristics, that is, orders of streams of a river network are depending on only its graph structure. Hence, given that some water sources correspond to one river mouth, the order in which sources are connected by stream determines orders of each stream. Ronald Shreve [40] noted this and called two networks *topologically identical* if they are tranformed to each other continuously in the plane projection, or *topologically distinct* if not. Based on this notion, Shreve published a statistical study [41] in 1974 which shows the most of randomly generated topologically distinct networks approximately obey Horton's law of stream numbers, stating "the law of stream numbers is indeed largely a consequence of random development of the topology of channel networks according to the laws of chance."

Moreover, James Kirchner wrote a critisism on Horton's law, showing further analysis of random networks [42]. Setting length and contributing are on each stream in addition to the randomly generated networks according to Shreve, his simulation also showed Horton's law of length and area of basin. However, the law also holded for biased selection of network topology, which meant it cannot distinguish between random and nonrandom sets of networks, and supported earlier arguments that the law must be an artifact of stream ordering methods, whereas Horton's law has been studied up to now for its importance on hydrological models [43–45].

2.1.2 Diameter exponent of biological transport network

Many transport networks can be found in organisms (Fig. 2.2); tree pumps up water from soil to leaf and transports product of photosynthesis, blood vessel network have crucial role for organism to distribute oxygen and nutrients and collect carbodioxyde and waste products throughout the body, and through bronchi which form deeply ramified structure, we can breathe and exchange carbodioxyde for oxygen. Despite the species and substances transported, they resemble one another as, for example, bronchial structure

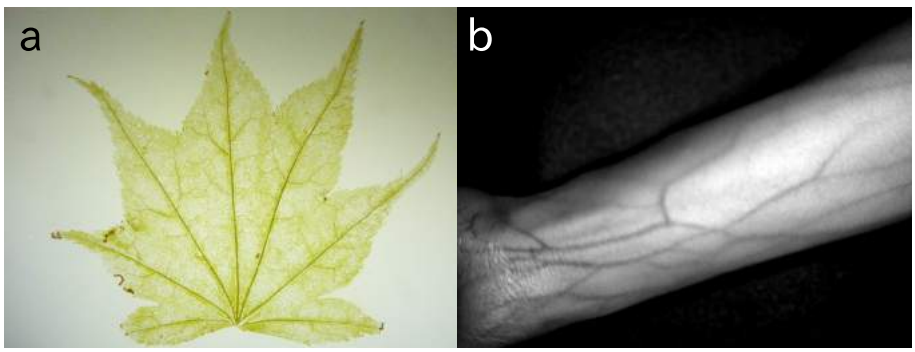

Fig. 2.2 Biological transport networks: (a) Leaf veins (b) Infrared picture of blood vessels of the author's right arm.

may be depicted as a tree in textbook on anatomy [46]. Actually, a rule on such branching structure exists and has been studied by various researchers.

The rule is on the relationship of diameters between parent vein and daughter veins on a branch, that is, given that a vein with diameter d_0 split into two veins with diameters d_1 and d_2, there exists a parameter n specific to the network such that

$$d_0^n = d_1^n + d_2^n. \tag{2.3}$$

The parameter n usually ranges from 2 to 3 and is called *diameter exponent* [47].

This law was firstly noted in the notebooks of Leonardo Da Vinci [48] as follows:

> "All the branches of a tree at every stage of its height when put together are equal in thickness to the trunk [below them]."

Although its literal interpretation is $d_0 = d_1 + d_2$, mordern interpretation of the sentence is, with consideration of his drawings, $d_0^2 = d_1^2 + d_2$ [47, 49]. He did not described actual measurement data but the law itself was not so wrong, as Cecil Murray proposed, in 1927, "2.5 power law of branching" based on his measurement [50].

In fact, Murray is famous for another diameter exponent $n = 3$. In his paper [51] published in 1926, he considered the morphology of blood vessels from the point of view of energy minimization. Consider a vein with radius r and length L. Then, assuming Hagen-Poiseuille flow [52], the flow rate Q by which blood of viscosity η flows with pressure difference ΔP is expressed as

$$Q = \frac{\pi r^4}{8\eta}\frac{\Delta P}{L}, \tag{2.4}$$

which means, conversely,

$$\Delta P = \frac{8\eta L}{\pi r^4}Q. \tag{2.5}$$

Hence, the friction loss $E_f = Q\Delta P$ is written as

$$E_f = \frac{8\eta L}{\pi r^4}Q^2, \tag{2.6}$$

so that larger radius makes lower friction energy. On the other hand, he introduced another cost E_b proportional to the volume, by which blood was maintained, that is, with a constant b,

$$E_b = b \cdot \pi r^2 L, \tag{2.7}$$

increasing with larger radius. Thus, E_f and E_b are in a situation of trade-off regarding r, and we can find the radius minimizing total enerygy $E_f + E_b$ by considering the condition in which the differentiation is equal to 0:

$$\frac{d}{dr}(E_f + E_b) = -\frac{32\eta L}{\pi r^5}Q^2 + 2\pi bLr = 0, \tag{2.8}$$

which gives a relationship

$$Q = 4\pi r^3\sqrt{b}. \tag{2.9}$$

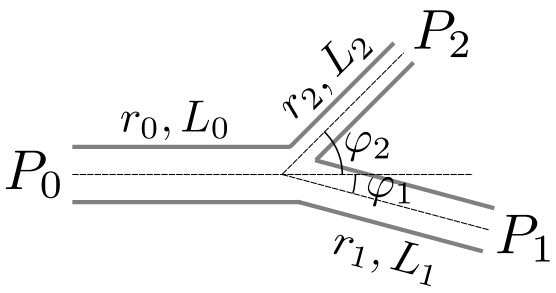

Fig. 2.3 A design of arteries transporting blood from fixed point P_0 to fixed points P_1 and P_2.

Therefore, given that a vein with radius r_0 and flow rate Q_0 is ramified into two veins with radii r_1 and r_2 and flow rate Q_1 and Q_2, conservation of flow rate $Q_0 = Q_1 + Q_2$ with the energy minimization leads to the cubic law of radii:

$$r_0^3 = r_1^3 + r_2^3, \tag{2.10}$$

which implies the diameter exponent $n = 3$ and often called *Murray's law*. Examinations of this law support the validity with small variances, estimating the diameter exponent n from 2.7 to 3.0 [17].

Murray applied this theory further to angle of branching, considering minimization of total volume cost of arteries connecting points of supply and demand [16]. Suppose that an artery with radius r_0 and length L_0 originated from a fixed source P_0 branches into an artery with radius r_1, length L_1, and angle φ_1 reaching a fixed point P_1 and another artery with radius r_2, length L_2, and angle φ_2 reaching another fixed point P_2 (Fig. 2.3), where each radius are optimized in the meaning of minimum energy above discussed, so that Eq. (2.9) holds on each artery for given flow rates Q_0, Q_1, and Q_2. Given that L_0 is lengthened to $L_0 + dL_0$ in the same direction, L_1 and L_2 are changed to $L_1 + dL_1$ and $L_2 + dL_2$, respectively, where

$$dL_1 = -dL_0 \cos\varphi_1, \tag{2.11}$$

$$dL_2 = -dL_0 \cos\varphi_2. \tag{2.12}$$

Hence, the change of the total volume is written as

$$dV = \pi dL_0(r_0^2 - r_1^2 \cos\varphi_1 - r_2^2 \cos\varphi_2). \tag{2.13}$$

When the geometry accomplish the minimized total volume, $dV = 0$ for the infinitesimal difference dL_0, which means

$$r_0^2 - r_1^2 \cos\varphi_1 - r_2^2 \cos\varphi_2 = 0. \tag{2.14}$$

In the same way, by considering infinitesimal extention of L_1 or L_2, we have

$$r_1^2 - r_0^2 \cos\varphi_1 + r_2^2 \cos(\varphi_1 + \varphi_2) = 0, \tag{2.15}$$

$$r_2^2 - r_0^2 \cos\varphi_2 + r_1^2 \cos(\varphi_1 + \varphi_2) = 0. \tag{2.16}$$

These equations on the radii and the angles enable us to find

$$\cos\varphi_1 = \frac{r_0^4 + r_1^4 - r_2^4}{2r_0^2 r_1^2}, \tag{2.17}$$

$$\cos\varphi_2 = \frac{r_0^4 + r_2^4 - r_1^4}{2r_0^2 r_2^2}, \tag{2.18}$$

$$\cos(\varphi_1 + \varphi_2) = \frac{r_0^4 - r_1^4 - r_2^4}{2r_1^2 r_2^2}. \tag{2.19}$$

Using notations $\alpha_1 = r_1/r_0$, $\alpha_2 = r_2/r_0$, and $\beta = r_2/r_1$ with the cubic law $r_0^3 = r_1^3 + r_2^3$, we see that

$$\cos\varphi_1 = \frac{1 + \alpha_1^4 - (1 - \alpha_1^3)^{4/3}}{2\alpha_1^2}, \tag{2.20}$$

$$\cos\varphi_2 = \frac{1 + \alpha_2^4 - (1 - \alpha_2^3)^{4/3}}{2\alpha_2^2}, \tag{2.21}$$

$$\cos(\varphi_1 + \varphi_2) = \frac{(1 + \beta^3)^{4/3} - 1 - \beta^4}{2\beta^2}. \tag{2.22}$$

These formulae, with an equivalent expression

$$\frac{r_0^2}{\sin(\varphi_1 + \varphi_2)} = \frac{r_1^2}{\sin\varphi_1} = \frac{r_2^2}{\sin\varphi_2}, \tag{2.23}$$

are also discussed for mathematical models of branching structure [53–56].

2.1.3 Transport network theory underlying scaling low

According to Schmidt-Nielsen [57], *scaling* is defined as a theory which "deals with the structural and functional consequences of changes in size or scale among otherwise similar organisms," that is, a theory on relationships between size and a variety of quantity. A scaling law on real organisms may be called *allometry* because it often treat nonisometric sizes [57], and usually biological scaling law is written as

$$Y = aW^b, \tag{2.24}$$

where Y is a biological characteristic such as daily sleeping time, ingestion rate, and metabolic rate, W is animal body mass, and a and b are constants [58]. Especially, the scaling law on metabolic rate stating the exponent $b = 0.74$ (usually denoted by 3/4) has attracted attention since firstly investigated by Kleiber [59] in 1932, covering so wide range of body mass that it is also known as *mouse-to-elephant curve*.

West *et al.* [1] explained this law from the view point of biological transport network. They started from three assumptions:

1. The network has a space-filling fractal-like branching pattern to supply the entire volume of the organism.

2. The final branch of the network is consisted of a size-invariant unit.
3. The energy required to distribute resources is minimized.

Because of the assumed fractal branching, every vein except for the final unit ramifies into the same number of veins, of which radius and length decrease geometrically according to the stage of branch. Then, by considering total flow which is proportional to metabolism, their theory derived the relationship between metabolic rate and body mass, where the exponent of body mass is determined by the fractal scale factors. Therefore, their theory can obtain not only the rule of metabolism but also other scaling law on biological variables by considering appropriate transport network structure.

In addition, Bejan [60] proposed another theory for the 3/4-power relation, dealing with transport network of heat. Although there are some explanations unrelated to network structure [58], it is natural to regard biological transport network to have enormous effects on physiology.

2.2 *Physarum polycephalum* as a model organism

2.2.1 Biology of slime mold

Slime mold is an organism characterized with the huge amoeboid stage showing vivid color and with the unique and beautiful fruit body specific to the species, recognized by human beings from long time ago. In Europe, a kind of slime mold, *Fuligo septica*, have been known as *flowers of tan* because it sometimes appeared on wasted tans, barks of certain trees used for tanning, which was written by Giambattista della Porta in 1588 [61, 62]. Some old documents of China may be older ones describing slime molds according to Kumagusu Minakata. He referred the volume 12 of *Miscellaneous Morsels from Youyang* (酉陽雑俎) written by Duan Chengshi (段成式) in about 860 and cited a sentence, "*Kwei shi* grows in shady damp ground and has a pale yellowish color, occasionally found and used for a cure of ulcers" (鬼矢生陰湿地浅黄白色或時見之主治悪瘡), stating that the word *Kwei shi* (鬼矢, literally *Demon's drops*) meant a slime mold, *Physarum gyrosum* [63–65]. In addition, he suggested that an old Chinese tradition that the blood of an innocent victim would reappear as sky-blue in color had an origin on an emergence of *Physarum gyrosum* [66] and when he prensented his collection to the Togu Palace, referred an even older literature *Lüshi Chunqiu* (呂氏春秋) written by Lü Buwei (呂不韋) around 240 BC and its sentence of volume 14, "Chang Hong died. Saved for three years, his blood became sky-blue" (萇弘死、藏其血三年而為碧) [67], which is, however, interpreted usually as "His blood became jasper (due to his loyalty)" [68], and a Chinese mycologist LI Yu proposed instead *Supplement to Medica* (本草拾遺) written by Chen Tsang-chi (陳藏器) in 739 as the earliest document describing slime mold [69]. Even modern people are sometimes amazed at the curious huge amoeba, as citizens of a suburb of Dallas saw unusual outbreak of *Fuligo septica* in 1973, regarding it as an *unidentified growing object* at first [65]. Surely slime mold is not so familiar compared with mushrooms consumed as ordinal food, but in Veracruz, Mexico, *Enteridium lycoperdon* is known as *feces of moon* (caca de luna), and fry of it is eaten by some residents [70].

In the words of biology, slime molds are eukaryotes classified into two class, Myxogastria (or Myxomycetes) and Dictyostelia, which are different in the cell behavior. To distinguish

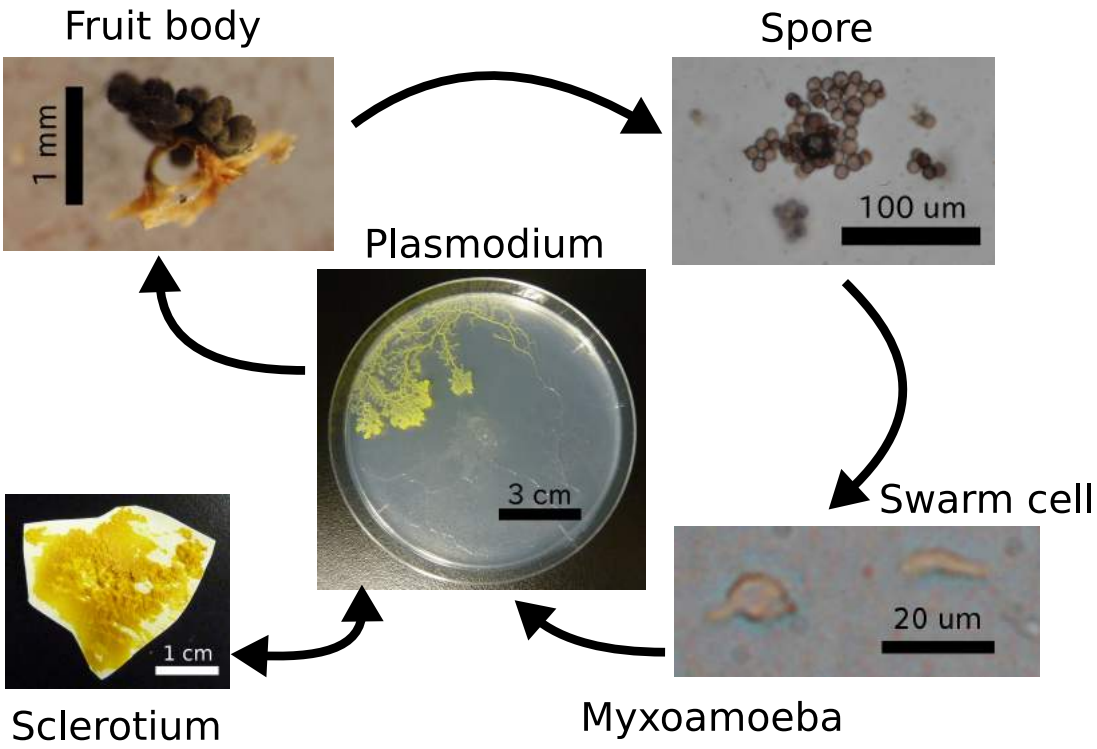

Fig. 2.4 A typical life cycle of Myxogastria. The pictures are *Physarum polycephalum*, taken by the author. Many sophisticated figures and descriptions of the life cycle can be found in literatures on Myxogastria [71–75].

them, Myxogastria is called *true slime mold* or *acellular slime mold*, and Dictyostelia is called *cellular slime mold*. This research treats a spieces of Myxogastria, *Physarum polycephalum*.

Fig. 2.4 shows a typical life cycle of Myxogastria. Spores in a fruit body are ordinary $5 \sim 15$ μm in diameter and drift in the air by, for example, blowing wind or touching animals. They start the germination under suitable conditions and produce one to four haploid motile cells, which tend to be an amoeboid form (called *myxoamoeba*) under drier condition but to be swarm cells with flagella in the presence of free water. Depending on environments, myxoamoebae and swarm cells can transform themselves into each other and especially under unfavorable conditions, form microcysts, developing a thin cell wall. These haploids have sexual types, and compatible pair of them fuses into diploid zygote. From the stage of zygote, cell division does not happen while nuclear division does, so that the cell become a large multinucleate organism which is called *plasmodium*. Plasmodium moves around and consumes bacteria. Although unsuitable conditions such as low temperature and desiccation induce the resting stage of plasmodia, *sclerotium*, it resumes its behavior as a plasmodium when favorable environments come. A matured plasmodium forms fruit body with some triggers such as strong lights and starvation, and the giant single cell are divided into spores to be the next generation.

The life cycle of Dictyostelia is similar to that of Myxogastria and was therefore considered to belong to Myxogastria in the first description by Oscar Brefeld [76]. However, Dictyostelia have the *pseudoplasmodium* stage instead of the plasmodium stage, which is

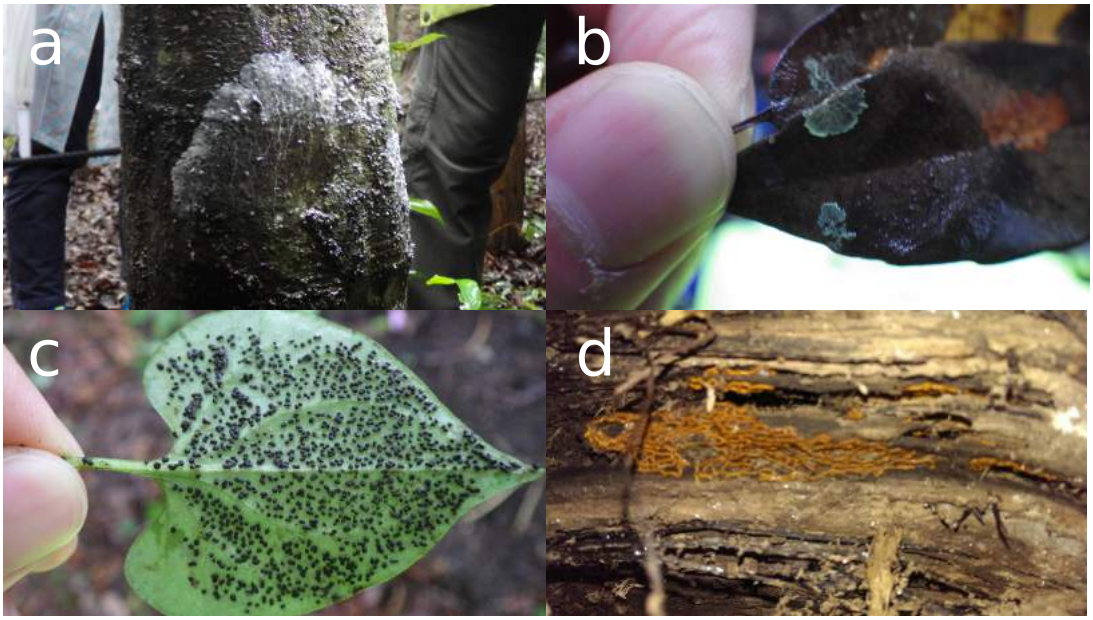

Fig. 2.5 True slime molds in nature. (a) A white plasmodium climing a trunk. (b) A yellow plasmodium moving on a fallen leaf. (c) *Didymium laccatipes* in the process of sporulation behind a leaf. (d) A fruit body of *Hemitrichia serpula*. Pictures (a), (b), and (c) were taken in Tsukuba botanical garden, and picture (d) was taken in the campus of Hokkaido University.

the main difference between Myxogastria and Dictyostelia.

The taxonomic position of Myxogastria has been controversial for a long time. Slime molds had been studied traditionally by botanists and treated as a kind of fungi. Heinrich Anton de Bary, however, distinguished them from fungi by giving a clearer definition of fungi in his textbook in 1866 [77]. Ernst Heakel's three-kingdom system which was published in 1866 also discriminated the two classes, classifying Myxogastria into the kingdom Protista and putting fungi in Nematophyta or Jnophyta of the kingdom Plantae [78]. Although five-kingdom system which Robert Harding Whittaker proposed in 1969 located Myxogastria in the kingdom Fungi again [79], the modified five-kingdom system published by Lynn Margulis and Karlene Schwartz in 1982 include Myxogastria in the kingdom Protoctista [80]. Now Myxogastria is mainly dealt with as a kind of protists. The international scociety of protistologits proposed a new classification system of Eukaryotes in 2005 [81] and revised it in 2012 [82], in which Myxogastria belonged to a super-group Amoebozoa of Amorphea.

The number of species of Myxogastria amounts to approximately 900 [72, 83], and the classification system of them is an on-going study, so that the way of classification varies between monographs on Myxogastria. While in nature, true slime molds are found usually as fruit bodies or a plasmodia like Fig. 2.5, a plasmodium itself hardly determine the species, but the morphology of a fruit body and its spore is the most important for the identification. Therefore, a plasmodium found in nature will be identificated after the sporulation. However, there are a variety of the morphology of plasmodium in fact, and classified into three types specific to species. *Phaneroplasmodium* is the most usual type

of plasmodium, forming a giant moving amoeba with anterior fan-shape structure and posterior vein structure. While phaneroplasmodium has color variety, *aphanoplasmodium* has thin transparent vein structure without frontal fan-shape margin, and the third type, *protoplasmodium*, forms colorless, veinless, and relatively small amoeba.

Physarum polycephalum, used in this study, is a species of Myxogastria widely used in laboratory studies due to easiness of culture. As the name suggests, it forms characteristic multi-headed fruit body with stalk, usually on dead wood, fleshy fungi or living plants, distributed in North America, South America, Hawaii, Europe, and Asia. The spores are $8 \sim 11$ μm in diameter and violaceous by transmitted light. The plasmodium is a typical phaneroplasmodium (Fig. 2.4) and mainly consists of protoplasm without cell wall. However, the protoplasm is sorrounded by plasma membrane, and moreover, hyaline glycocalyx exists in further outside of the plasma membrane. This membrane structure is not stiff but vulnerable whereas rapidly reproduced. Hence, even if a plasmodium is severed into two bodies, each can survive as an individual, regenerating the membrane structure. Conversely, contact of two plasmodia of identical genotype cause cell fusion, though that of different genotypes has a lethal interaction [84].

Protoplasm is classified into *plasmasol*, solled protoplasm flowing through vein, and *plasmagel*, gelled protoplasm constituting wall of vein. Plasmagel contains actin and myosin, which produce rhythmic contraction and relaxation originating flow of plasmasol [75, 85], which alters its direction according to the rhythm of contraction and relaxation, so that it is named *shuttle streaming*.

2.2.2 Information processing of *Physarum polycephalum*

Usual researches on biological information processing deal with neuronal circuits or behaviours of animals having nervous system, while even unicellular organisms having no nervous system can perform some kinds of information processing. For example, *Paramecium caudatum* can perform associative learning for light and temperature and memory of space where it is confined [86]. In addition, when the organism arrives at an end of a thin capillary, it manages to turn its direction after some trials by bending the body, reducing the number of tries with experiences of the bending turn [87], which can be interpreted as a kind of learning. Kunita *et al.* reported that if the capillary was so narrow that *Paramecium* could not even bend the body, it swimmed back and forth, increasing the length of swimming with the number of trials [88]. They proposed a mathematical background of this behavior by considering membrane potential which is concerned with the direction of swimming. Spacial memory of *Tetrahymena* is also modelled with dynamics of ion channels [89]. Of course, plasmodium of *Physarum polycephalum* can show kinds of information processing, as written in followings.

In 2000, Nakagaki *et al.* reported pioneering work on information processing of slime mold, which stated that *Physarum polycephalum* solved maze [11]. In their experiment, pieces of plasmodium were put on a maze which was formed by plastic films on agar. Each plasmodium expanded its own body and coalesced one another, so that the maze was filled with one plasmodium. Then, food sources were put on start and goal point of the maze, driving the plasmodium to gather at the foods and make veins to distribute digested nutrients. The experiment finally settled in a state where allmost all parts of plasmodium evacuated the maze and aggregated on the food sources with veins connecting

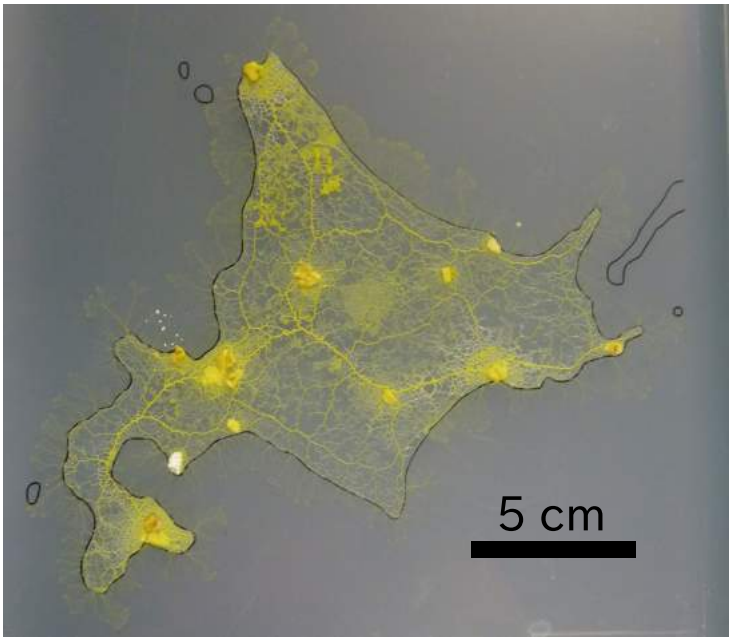

Fig. 2.6 Transport network connecting cities in Hokkaido produced by *Physarum polycephalum*. Plastic film on agar forms the shape of Hokkaido and oat flakes are put on place of main cities.

the start and the goal, which was, at the same time, a solution of the maze. Although at first, the word "primitive intelligence" the authors used was somewhat controversy [90]. now many researchers deal with *Physarum polycephalum* as a model organism of biological information processing.

One of the reasons why slime mold solving task to connect food sources attracts attentions is that slime mold seems to create veins optimising trade-offs. In the maze experiment, slime mold tend to preserve shorter path and extinguish longer path if there are some candidates for the solution, while sometimes both shorter and longer path are remained, and it follows that path-finding of slime mold has multi-functionality of cost minimization and fault torelance for disruption of vein. This ability to solve trade-offs is more clearly found and quantified by tasks where slime mold connects multiple food sources [9, 91, 92]. Moreover, environmental cost can be set on experiment to connect food sources by illuminating light, which is unfavorable for plasmodium, in proportion to the cost, and slime mold can form vein network with consideration of this cost of location [9, 10]. This multi-functionality is exploited in some studies for designing rail-way or road networks to compare the real ones [9, 93, 94] (Fig. 2.6 shows an example of transport network desined by slime mold connecting cities in Hokkaido). One of proposed mechanisms underlying these delelopment of vein network is current-reinforcement dynamics, which is described in detail in 2.2.3.

In addition to connecting tasks, various biological information processings were implemented using slime mold. Saigusa *et al.* demonstrated that plasmodium changes its migrating speed with anticipating periodic enviromental change, and proposed its mathematical model by considering chemical oscillations in protoplasm having different periods [95]. Takagi *et al.* reported indecisive behavior of locomoting slime mold and modelled

the dynamics based on a reaction-diffusion system called Gray-Scott model [96], which was modified to be more realistic by Ueda *et al.* [22]. Aono *et al.* composed a device in which slime mold solve a famous combinatorial problem, the travelling salesman problem [97]. These studies imply that even an unicellular organism has mechanisms to solve complex problems which usually human treats.

2.2.3 Current-reinforcement model for vein network of *Physarum polycephalum*

2.2.3.1 Outline

As a mechanism of the desining ability of slime mold, Tero *et al.* [8] proposed a simple but potent dynamics, *current-reinforcement*, which represents plasmodium as a random meshwork of tubular channels and develops the diameter of tubes according to a simple rule. Roughly speaking, the rule is "flows more, gets thicker" and "flows lesser, gets thinner," like the first law of Jean-Baptiste Lamarck published in 1809 [98]:

> "In every animal which has not passed the limit of its development, a more frequent and continuous use of any organ gradually strengthens, develops and enlarges that organ, and gives it a power proportional to the length of time it has been so used; while the permanent disuse of any organ imperceptibly weakens deteriorates it, and progressively diminishes its functional capacity, until it finally disappears."

Compared with other models [99–102], it is characteristic of current-reinforcement dynamics to have an expression as a differential equation and consider fluid dynamics.

The model assumes that the protoplasmic stream is Hagen-Poiseuille flow, laminar flow in cylinder. Under this assumption, velocity $v(x)$ at a point of distance x from center of cylinder with radius r is given as

$$v(x) = \frac{r^2 - x^2}{4\eta L}\Delta P, \tag{2.25}$$

where η, L, and ΔP are the viscosity of protoplasmic sol, the length of the vein, and the applied pressure difference, respectively [103]. Hence, the flow rate Q is obtained as

$$Q = \int_0^{2\pi}\int_0^r v(x)x\,dx\,d\theta = \frac{\pi r^4}{8\eta L}\Delta P. \tag{2.26}$$

As experimental facts on protoplasmic streaming of plasmodium, studies in 1950's using cinematograph stated that velocity profile across diameter of vein is a parabola whose apex is flattened [104], although in 2009, imaging technique of Bykov *et al.* obtained parabolic velocity profile around the phase of top speed of shuttle streaming [105], which supports the assumption of Hagen-Poiseuille flow.

Another assumption of current-reinforcement dynamics is volume conservation. Suppose that vertices i and j, at which pressure is P_i and P_j, respectively, are connected by channel ij, with uniform diameter r_{ij} and length L_{ij}. Flow rate Q_{ij}, with consideration of direction of flow, is now defined as

$$Q_{ij} = \frac{\pi r_{ij}^4}{8\eta L_{ij}}(P_i - P_j). \tag{2.27}$$

Then, volume conservation is assumed at vertex i as

$$\sum_j Q_{ij} = J_i, \tag{2.28}$$

where J_i is a nonzero constant if vertex i is a source or sink of current, and J_i is zero otherwise. In addition, J_i is assumed to satisfy

$$\sum_i J_i = 0 \tag{2.29}$$

for feasibility of finding flows (see 2.2.3.2).

Here, letting D_{ij} denote the conductivity per length[*1] $\pi r_{ij}^4/8\eta$ which means

$$Q_{ij} = \frac{D_{ij}}{L_{ij}}(P_i - P_j), \tag{2.30}$$

we set the current-reinforcement rule:

$$\frac{\mathrm{d}D_{ij}}{\mathrm{d}t} = f(|Q_{ij}|) - D_{ij}, \tag{2.31}$$

where f is a monotonically increasing continuous function satisfying $f(0) = 0$. Essentially, Eq. (2.31) is a differential equation of radius r_{ij} because we assume constant viscosity η and length L_{ij}.

If the current sources and sinks with J_i are given, and L_{ij} and r_{ij} of all channels are known, all Q_{ij} can be determined as written in 2.2.3.2. Once there is flow on the network, the current-reinforcement rules modify the thickness of each channel in the next time step according to the flow it is carrying.

Eq. (2.31) contains two antagonistic components: $f(|Q_{ij}|)$ represents a thickening factor that increases with the current, whilst $-D_{ij}$ is a intrinsic thinning factor. Thus, the thickening component dominates for a channel with a larger current, and the thinning

[*1] Note the concatenation rule of conductivity. Suppose that vertices $1, 2, ..., N$ are connected in straight with the same vein with radius r, length L, and conductivity $D = \pi r^4/8\eta$, and $J(i)$ is equal to $-J_0$ for $i = 1$, J_0 for $i = N$, and 0 for else, so that

$$Q_{i+1,i} = D(P_{i+1} - Pi)$$

for $i = 1, ..., N-1$. From the volume conservation, we have

$$Q_{N,N-1} = \cdots = Q_{21} = J_0.$$

Given that $P_1 = 0$,

$$P_N = \frac{(N-1)J_0}{D}.$$

Hence, as one concatenated vein connecting nodes 1 and N,

$$Q_{N1} = J_0 = \frac{D}{N-1}(P_N - P_1),$$

which means $D_{N1} = D/(N-1)$. Thus, concatenation rule for cunductivity is not simple sum, so that the total conductivity is given by D/L for conductivity per length D and length L.

effect dominates for one with smaller current at each time step. The complete temporal evolution of the network is then calculated iteratively with the updated conductivities. Regarding food sources as sources and sinks, the current-reinforcement dynamics reproduces vein networks of slime mold after the iteration [8–10].

2.2.3.2 Theory to find flows in vein network

To simulate the current-reinforcement model, we need to find flows Q_{ij} for given D_{ij}, L_{ij}, and quantities of source or sink in every node. Analogy of electric circuit is useful to solve this problem because the proportional relationship between flow and pressure corresponds to Ohm's law where current I is proportional to applied voltage V with coefficient G, conductance, that is,

$$I = GV, \tag{2.32}$$

while usually, the equation is written with resistance $R = 1/G$ as

$$V = RI. \tag{2.33}$$

For given voltage or current source and resistances on edges, circuit theory can find how much current flows in each edge [106]. The problem to find flow rates in a vein network contains informations on source or sink and hydrodynamic conductivity D_{ij}/L_{ij} which correspond to current source and hydrodynamic conductivity, respectively, so that the circuit theory is applicable.

Here, terminology of graph theory is used to deal with a vein network as a directed graph. A *directed graph* $G = (V, E)$ is an ordered pair of a finite set V of which element is called *vertex* and a finite set E of which element $e = (u, v)$ is called *edge* and defined as an ordered[*2] pair of two elements $u, v \in V$, that is, the edge e connect verticese u and v. If E does not contain any edges which connect an identical vertex and any two edges which connect the same pair of vertices, the graph $G = (V, E)$ is called *simple*, and if the graph is not separated but connected with edges as a whole, the graph is called *connected*. We regard a vein network as a simple, connected, and directed graph.

To implement the settings of the problem, let $U(v)$ denotes pressure at a vertex v. Then, pressure difference $P(e)$ on $e = (u, v)$ is expressed as

$$P(e) = U(u) - U(v). \tag{2.34}$$

Given that $D(e)$ is the hydrodynamic conductivity of the vein e, the flow $Q(e)$ is calculated as

$$Q(e) = D(e)P(e). \tag{2.35}$$

If a vertex v is a source of quantity $J(v)$ (negative $J(v)$ means sink), sum of outflow subtracted by sum of inflow must be equal to $J(v)$, that is,

$$\sum_{e \in \mathrm{From}(v)} Q(e) - \sum_{e \in \mathrm{To}(v)} Q(e) = J(v), \tag{2.36}$$

[*2] Definition neglecting the order of vertices of edge means simply *graph*

where

$$\mathrm{From}(v) = \{e \in E | e = (v, u)\}, \tag{2.37}$$

$$\mathrm{To}(v) = \{e \in E | e = (u, v)\}. \tag{2.38}$$

By summing Eq. (2.36) for all $v \in V$, we have a constraint on $J(v)$ for which

$$\sum_{v \in V} J(v) = 0. \tag{2.39}$$

We consider these equations using vectors and matrices. Consider orders on V and E so that we can list all of the elements of V and E by $v_1, ..., v_N$ and $e_1, ..., e_M$. Then, vector $\mathbf{U}$ and $\mathbf{P}$ is defined as

$$\mathbf{U} = \begin{pmatrix} U(v_1) \\ \vdots \\ U(v_N) \end{pmatrix}, \tag{2.40}$$

$$\mathbf{P} = \begin{pmatrix} P(e_1) \\ \vdots \\ P(e_M) \end{pmatrix}. \tag{2.41}$$

Because $P(e)$ of $e = (u, v)$ is a linear combination of $U(u)$ and $U(v)$, there exists a matrix A such that

$$\mathbf{P} = {}^tA\mathbf{U}, \tag{2.42}$$

where ${}^tA$ means the transpose matrix of A. The $N \times M$ matrix A, of which element A_{ij} is expressed as

$$A_{ij} = \begin{cases} 1, & e_j \in \mathrm{From}(v_i), \\ -1, & e_j \in \mathrm{To}(v_i), \\ 0, & \text{else}, \end{cases} \tag{2.43}$$

is called *incidence matrix*, of which rank is equal to $N-1$ and any row is linearly depencent by the others [107]. In fact, the pressure has a degree of freedom on its origin. Assuming v_N is the only one sink and $U(v_N) = 0$, the Nth column of A effects nothing on $\mathbf{P}$. Under this assumption, we let $\mathbf{U}_r$ and A_r be the vector $\mathbf{U}$ without the Nth element and the matrix A without the Nth column, so that

$$\mathbf{P} = {}^tA_r\mathbf{U}_r. \tag{2.44}$$

Next, considering a diagonal matrix

$$D = \begin{pmatrix} D(e_1) & & 0 \\ & \ddots & \\ 0 & & D(e_M) \end{pmatrix}, \tag{2.45}$$

the flow vector $\mathbf{Q}$ is written as

$$\mathbf{Q} = D\mathbf{P}. \tag{2.46}$$

Furthermore, using A_r, we see that

$$A_r \mathbf{Q} = \mathbf{J}_r, \tag{2.47}$$

where

$$\mathbf{J}_r = \begin{pmatrix} J(v_1) \\ \vdots \\ J(v_{N-1}) \end{pmatrix}. \tag{2.48}$$

Combining Eqs. (2.44), (2.46), and (2.47), we have

$$A_r D^t A_r \mathbf{U}_r = \mathbf{J}_r. \tag{2.49}$$

Because the $N-1 \times N-1$ matrix $A_r D^t A_r$ is full rank, we can find $\mathbf{U}_r$ by

$$\mathbf{U}_r = (A_r D^t A_r)^{-1} \mathbf{J}_r. \tag{2.50}$$

Finally, the flow vector $\mathbf{Q}$ is calculated by Eq. (2.46).

Chapter 3

Materials and Methods

3.1 Culture of plasmodia

Plasmodia of *Physarum polycephalum* have been used long time for many kinds of biological and, especially in recent time, behavioral experiment because of the easiness of culture. Methods to culture large quantities of plasmodia had been established no later than 1931, the time when Frank Howard reported a laboratory cultivation of plasmodia on agar with oats [108]. In 1936, William Camp showed another method using gauze or filter paper as substrate [109]. While these methods do not mean pure culture, that is, the chamber can be, strictly speaking, contaminated by other bacteria, some pure culture methods have been devised [110–112].

Our culture method, as shown in Fig. 3.1 is essentially the same with that of Howard and needs a dark place of which temperature is controlled to be around 27 °C. First, pieces of filter paper on which sclerotia formed are put on 1% (w/v) agar (S-7, Ina Food Industry) and sprayed water to be moistened. After overnight storage, plasmodia move around on the agar. Then, the part of the agar on which filter papers were put is cut off, and oat meal flakes (Original flavor, Quaker) are strewed in proportion with the mass of plasmodia few times in a day. When the agar is filled with oat flakes, and all of them are covered by the yellow plasmodia, we cut the plasmodia together with the agar substrate into some pieces and put them on some new agar plates. After the transplanted plasmodia spread on the new agar, the part of the agar on which the old agar were put is cut off, and feed the plasmodium with oats. This cycle gives quick proliferation of plasmodia.

Plasmodia can be transformed by desiccation to sclerotia, which is convinient to store for a period in which no experiment is conducted. For the desiccation, well-grown plasmodia just before transplantation are put in the bottom of a bucket, inside of which wet pieces of filter paper (No. 50, Advantec) are pasted on the wall. Then, the bucket is stored with its lid in the dark until the plasmodia climb the wall up to end of the filter paper. The plasmodia, together with the paper, are moved into a cardboard box and desiccated slowly. Dried completely in few days, they transform themselves to sclerotia, and we save the sclerotia in a dark and dried place.

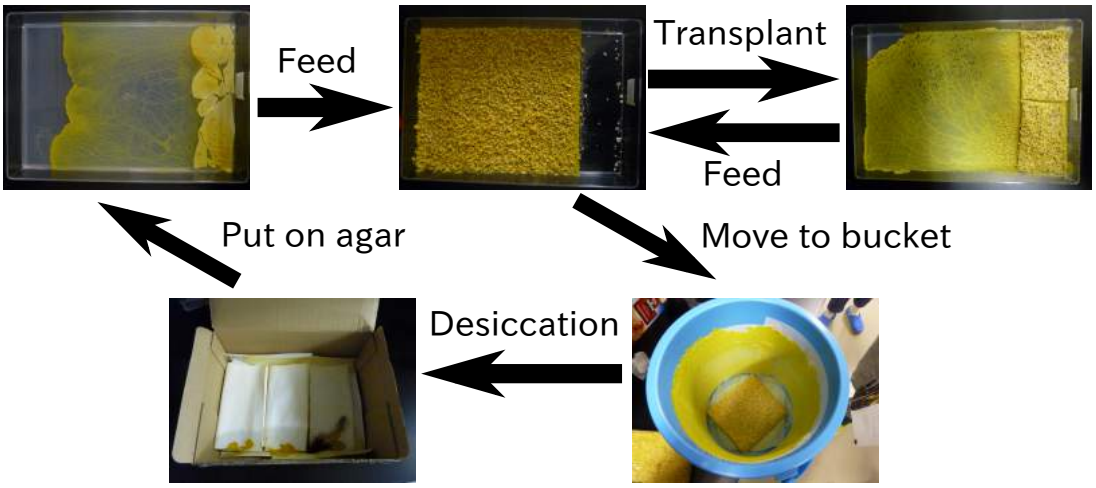

Fig. 3.1 Laboratory-culture cycle of plasmodia of *P. polycephalum*. The size of the agar tray is 350 mm × 255 mm × 60 mm, and the diameter of the bucket is 310 mm.

3.2 Establishment of an evacuation network from a confined space

In this study, we prepared protoplasmic sheets which consist of only protoplasm and have no network structure, to observe a development of a vein network from a uniform state. For that purpose, protoplasm was obtained by excision of thick veins of actively growing plasmodium, and sandwiched between glass plates with a gap 0.12∼0.17 mm. Within a few seconds, the protoplasm gelled to give a uniform sheet. The sheet was transferred to a small arena cut out from plastic film, and placed on agar (See panels `init` and `0h` in Fig.4.1). Food was placed on the exit to encourage the slime mold to evacuate the arena and promote formation of the vein network. A range of arenas with different shapes were tested including circular (C, 10 mm diameter), rectangular (R1, 6 mm × 17.5 mm; R2, 7.5 mm × 14.5 mm; R3, 10 mm × 10 mm; R4, 14 mm × 7.3 mm; R5, 20 mm × 5 mm), or irregular (A).

Time-lapse images were obtained with transmitted light. The thickness was estimated as $h = -\log(I/I_0)$ according to the Beer-Lambert law, where I and I_0 were the intensities of transmitted and incident light. Although some automated methods have been proposed for detecting and extracting tubular networks [113–115], the network morphology was obtained by manually tracing the main veins on the 2-dimensional map of h because of existence of many unclear veins in emergence. Experiments were repeated five times for the circular and rectangular shapes, and three times for the irregular shape. To analyze the time-course of changes in h, the map of h was processed initially with a averaging filter of radius 350 μm to give h_{av}. From the locally averaged thickness h_{av}, we estimated the evacuation time-constant τ and the initial value h_0 of $h_{\mathrm{av}} = h_0 \exp(-t/\tau)$ for each pixel so that the squared error was minimized.

3.3 Quantitative analysis of the network organisation and transport capacity

The space-filling properties of the network were estimated from the maximum distance between every pixel in the arena and the nearest pixel on the manually extracted network of thick veins to give the Hausdorff distance. Mathematically, the Hausdorff distance between two subsets A and B of a metric space (X, d) is defined as

$$d_H(A, B) = \max\{\sup_{x\in A}\inf_{y\in B} d(x, y), \sup_{y\in B}\inf_{x\in A} d(x, y)\}.$$

Given that A is the arena and B is the traced network,

$$\sup_{y\in B}\inf_{x\in A} d(x, y) = 0$$

because $B \subset A$. It follows that

$$d_H(A, B) = \sup_{x\in A}\inf_{y\in B} d(x, y),$$

where $d_H(A, B)$ represents the maximum distance between every pixel in the arena and the nearest pixel on the network. To compare results between the different arena shapes, the Hausdorff distance was divided by the maximum distance within the arena to give the normalized Hausdorff distance.

The predicted performance of the network was estimated from the hydraulic conductivity of each vein. Assuming Hagen-Poiseuille flow, the conductivity of each segment was estimated from manual measurements of the thickness and length, and concatenated to give the hydrodynamic conductivity (HC) for any point in the network to the exit point.

3.4 Validation methods for Murray's law

As an examination of Murray's theory, diameters and branch angles of 57 nodes were manually measured from the set of circular networks. d_0 was defined as the maximum diameter out of the 3 veins at the branch and d_1 and d_2 the daughter diameters which ramify with angles φ_1 and φ_2 (Fig. 3.4). The diameter exponent n was then calculated to satisfy the relationship $d_0^n = d_1^n + d_2^n$ for each junction.

Note that errors in diameters cause an asymmetric error in the exponent n by this calculation. For example, consider a junction in which $d_1 = d_2 \geq d_0/2$, so that $d_0^n = 2d_1^n$. We can solve n for this case as

$$n = \frac{\log 2}{\log d_0 - \log d_1}, \tag{3.1}$$

and it follows that

$$\frac{\partial n}{\partial d_1} = \frac{\log 2}{d_1(\log d_0 - \log d_1)^2} > 0, \tag{3.2}$$

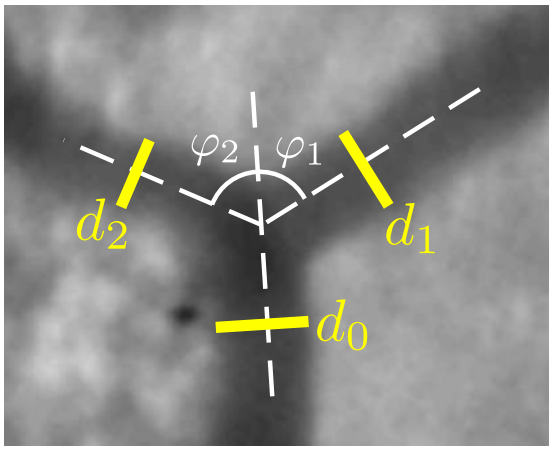

Fig. 3.2 Measurement of branching geometry.

$$\frac{\partial^2 n}{\partial d_1^2} = \frac{\log 2}{d_1^2 (\log d_0 - \log d_1)^3} \left(2 - \log \frac{d_0}{d_1}\right) > 0. \tag{3.3}$$

Therefore, given that the measurement of d_1 gives a value of an interval $[d_1 - \delta, d_1 + \delta]$, the calculated exponent takes a value of an interval $[n - \delta_1, n + \delta_2]$ where $0 < \delta_1 < \delta_2$. In other words, the distribution of the calculated exponent is asymmetric, having a long tail on the right side, and thus the mean of the calculated exponent is not appropriate for the estimation of n.

To estimate the exponent n fairly, we need to transform n to another variable of which distribution is symmetric at least. Suwa *et al.* [116], on a research of the exponent for arteries, discussed the same problem and found that arctangent transformation was the most effective way for this purpose, that is, the distribution of $\arctan n$ was similar to a normal distribution. Then, instead of n, $\arctan n$ and its confidence interval were estimated by a usual statistics for a normal distribution, followed by estimation of n by the inverse transformation. We utilised this method for our data.

Chapter 4

Results

4.1 Emergence of vein network and evacuation kinetics

4.1.1 Evacuation networks form rapidly and remain topologically stable

Plasmodial sheets of *Physarum* placed in a confined circular arena rapidly expanded to fill the available space to give a near uniform thickness (Fig. 4.1, 0-1h). The introduction of a food resource at the exit stimulated evacuation of the slime mold from the arena through an emerging network of veins that ramified throughout the arena (Fig. 4.1, 2-9h). Once the initial network of thicker veins was visible, the topology remained stable throughout the evacuation period. The flux of protoplasm flowing through the branching network and thence out the arena was apparent from the almost uniform reduction in thickness of the plasmodium, until about 10h when the thinnest parts become resolved as a very fine network (Fig. 4.1, 10-14h). Similar observations were made on all replicates for each different shape of arena ($n = 5$ for the circular and the rectangular shapes, $n = 3$ for the irregular shape).

4.1.2 Evacuation kinetics through the vein network are similar across entire space

The near uniform reduction in thickness observed across the arena, implied that the rate of protoplasm removal was similar for all parts of the system irrespective of the distance to the exit. In fact, line-profile analysis shown in Fig. 4.2 shows homogeneous decrease along the monitored lines. Moreover, to quantify the rate of removal, the locally averaged change in cell thickness was measured from inter-vein regions adjacent to the exit (Fig. 4.3, A), mid-way away (Fig. 4.3, B), and nearly opposite the exit (Fig. 4.3, C). Although the euclidean distance to the exit point varied by a factor of four, the rate of protoplasmic removal was almost identical and fitted well by exponential decreasing (Fig. 4.3, black solid line). We therefore calculated the best-fit exponential to the time-series for each pixel and mapped the time-constant of the decay across the whole arena (Fig. 4.4), where a consistent value around 7 hour fills the inter-vein regions.

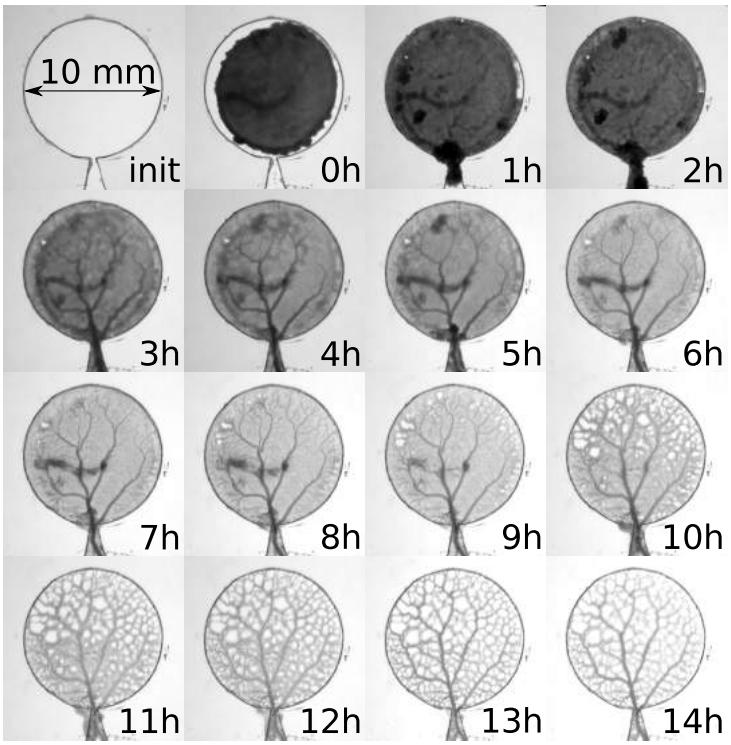

Fig. 4.1 Time course images following the development of a veination network by *Physarum* during evacuation from a confined circular arena.

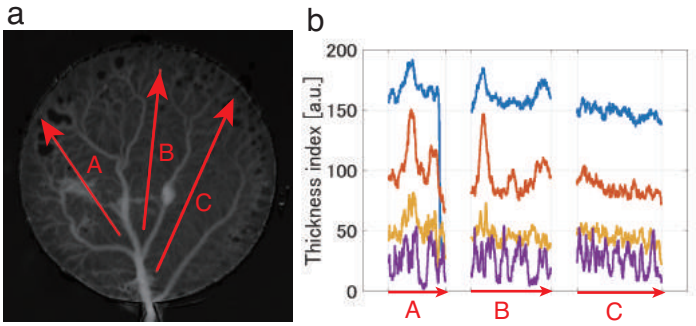

Fig. 4.2 Profile of plasmodial thickness along the monitored lines at times 0 (blue line), 4 (orange), 9 (yellow) and 14 (violet) hours after introducing the exit.

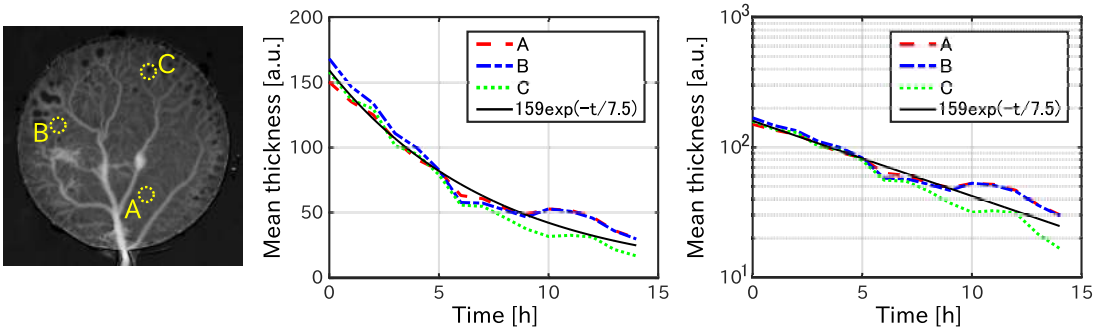

Fig. 4.3 Changes in the thickness of the plasmodium over time, monitored at three different inter-vein regions (left, A, B, and C). The plots show the time courses for the three points in addition to exponential fitting $159e^{-t/7.5}$ to the three lines with linear y-axis (middle) and logarithmic y-axis (right).

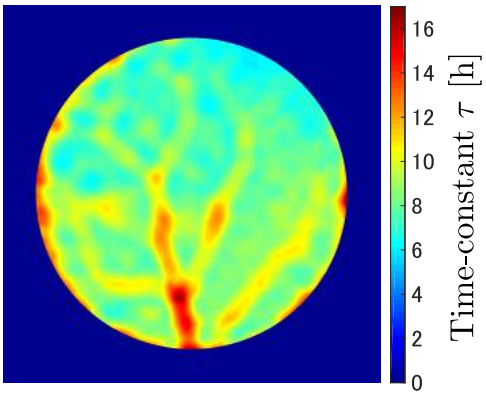

Fig. 4.4 Map of time-constant τ by which time development of thickness $h(t)$ in every point of arena is fitted to exponential formula $h(t) = h_0 e^{-t/\tau}$ where h_0 is another estimated parameter.

4.1.3 Evacuation is adaptive to space

To determine whether this organised behaviour was a consequence of using a circular arena or represented a general adaptive property of the network to achieve efficient protoplasmic movement and redeployment, the same experiments and analyses were conducted for rectangular arenas that differed in aspect ratio, and an arena with a more complex shape. As Fig. 4.5 and 4.6 show the results for a rectangle (6 mm × 17.5 mm) and an irregular shape, respectively, the networks developed as the drainage of body mass, and the line-profile analyses indicated that the evacuation kinetics was independent of distance from the exit. Moreover, time-constant analysis demonstrated remarkably consistent time-constants of around 8 hour for the rectangular shape (Fig. 4.5) and around 15 hour for the irregular shape (Fig. 4.6c) in the inter-vein regions. That is, the kinetics of evacuation are almost identical across the whole arena, irrespective of the arena shape.

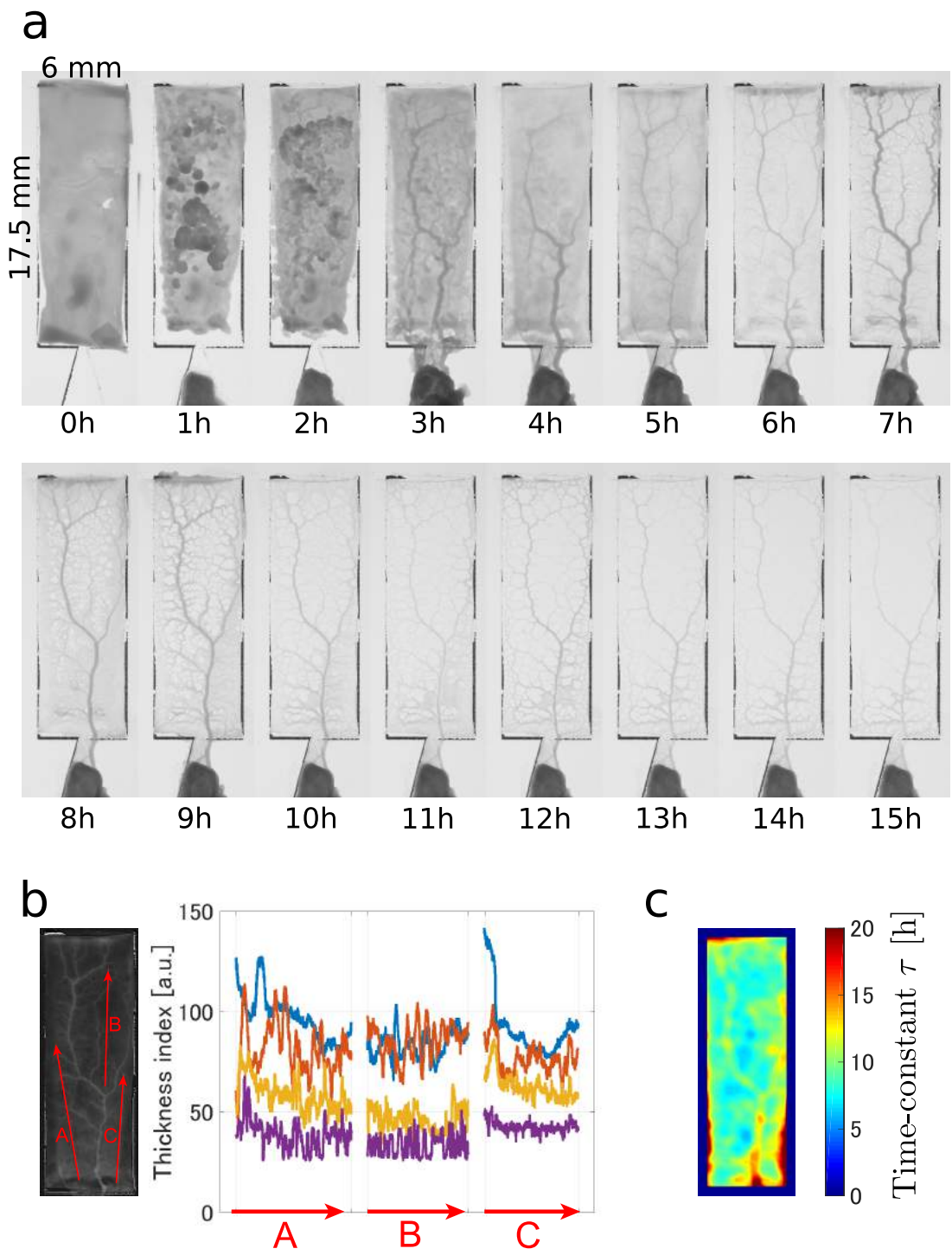

Fig. 4.5 Evacuation network emerging in a rectangular shape (6 mm × 17.5 mm). (a) Time-lapse images of evacuation. (b) Line-profile analysis. (c) Time-constant map.

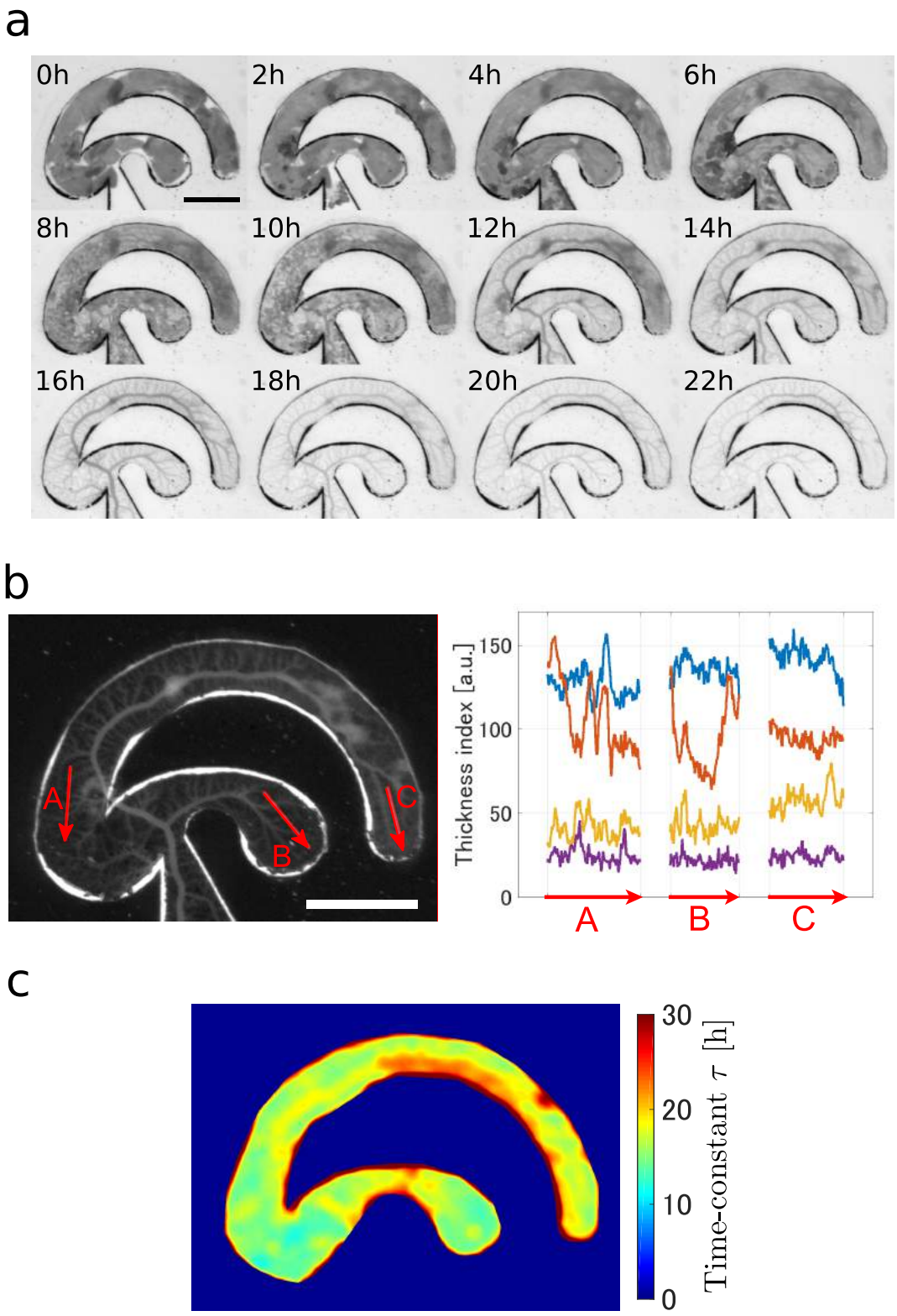

Fig. 4.6 Evacuation network emerging in an irregular shape (scale bar: 5 mm). (a) Time-lapse images of evacuation. (b) Line-profile analysis. (c) Time-constant map.

We infer from these results that the spatial disposition of the vein network that emerges during network formation, and the variation in thickness combine to service all regions of any shaped arena equally well.

4.1.4 Evacuation networks cover space effectively

Fig. 4.7 shows the vein networks extracted manually from a frame of each experiment, at which slime mold is evacuating from the arena through the developed vein network. To quantify how well the vein network serviced the entire space, the maximum distance from any point in the arena to the vein network was calculated as the normalised Hausdorff distance for each arena shape. Values were uniformly small in comparison to the extent of the available space, ranging from 0.1 to 0.2 (Fig. 4.8). This means that the main veins were distributed almost uniformly over the arena so that there were no isolated regions far from any vein.

4.1.5 Variation in network vein thickness gives similar hydrodynamic conductivity with distance

Whilst movement of material to the veins is reflected in the normalised Hausdorff distance, movement within the network depends on the thickness and hierarchical branching pattern of the vein segments, and the pressure gradients driving flow. Thus, flow from any point in the network to the exit is governed by the hydrodynamic conductivity (HC) of the pathway to the exit, which can be estimated from the physical dimensions of the veins themselves, and any variation in the actin-myosin contraction system present throughout the plasmodium. Interestingly, the measured hydrodynamic conductivity was similar for

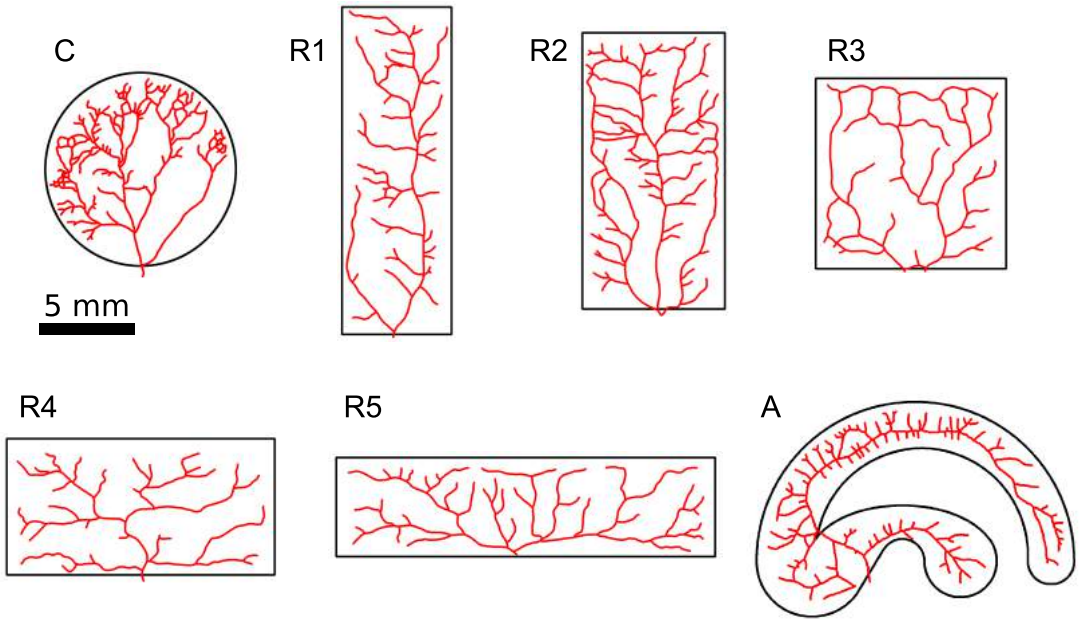

Fig. 4.7 Manually extracted evacuation network emerging in arenas.

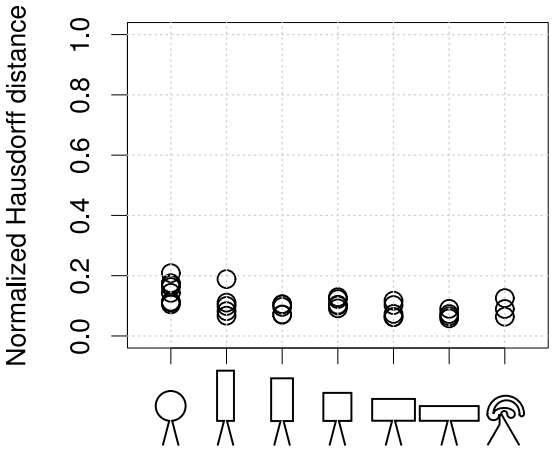

Fig. 4.8 Normalized Hausdorff distance for networks formed in each arena shape. The shapes tested are illustrated along the abscissa: from left to right, circle, tall rectangles, square, wide rectangles, and an irregular shape. The exit is located at the bottom of shapes, indicated by the trapezoid channel. ($n = 5$ for the circular and the rectangular shapes, $n = 3$ for the irregular shape).

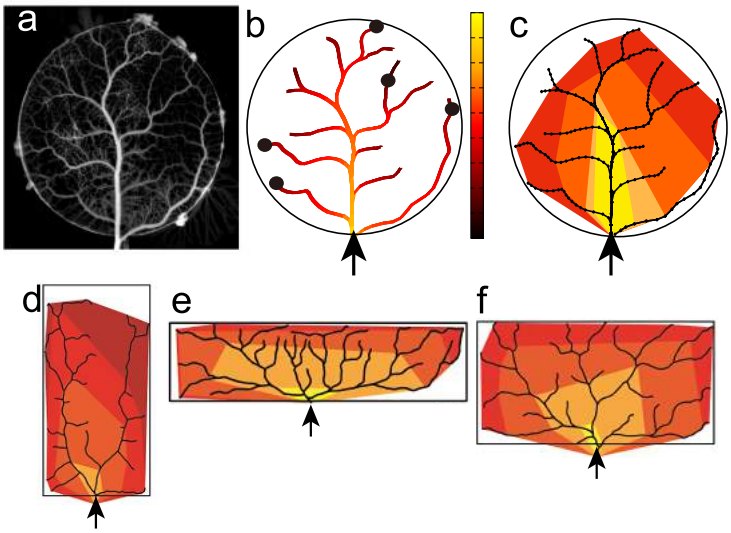

Fig. 4.9 Hydrodynamic conductivity of vein-network observed in the confined circular shape. (a) Thickness image of vein-network in the circle with diameter 1 cm. (b) Hydrodynamic conductivity along the main vein-network. A certain value of same HC was marked by the black dots on the network near the boundary of confined space. (c) Convex envelop for the dots marked in the figure b. (d, e, f) The same analysis on other shapes. Arrows indicate the location of exit.

peripheral points in the network (Fig. 4.9), and varied much less than the physical distance to the exit with position in the arena. The HC contours match the different arena shapes and help to explain the constant evacuation rate.

4.2 Examination of Murray's theory

4.2.1 Thickness relationship before and after a bifurcation

We infer from the consistency of the measured hydrodynamic conductivity that the branching pattern and parent-daughter vein thickness ratio at each bifurcation junction were likely to conform to a scaling relationship. In other transport systems dominated by viscous drag, Murray's Law predicts a cubic exponent according to Eq. (1.1), whilst networks with larger vessels follow an area preserving relationship.

In fact, as Fig. 4.10 shows a plot of $d_1^3 + d_2^3$ versus d_0^3 for the 57 three-way junctions present in the networks grown in the circular arenas, there are positive correlation (Pearson's $r = 0.946$). Moreover, parameter estimation of linear model $d_1^3 + d_2^3 = a + bd_0^3$ by a non-parametric method (Passing-Bablok regression [117–119]) shows 95% confidence intervals $[-2.85 \times 10^5, 5.19 \times 10^5]$ for a and $[0.945, 1.11]$ for b, including identical condition ($a = 0$ and $b = 1$) and supporting Murray's law.

As a further analysis, diameter exponent was calculated for each branches as the histogram is shown in Fig. 4.11a. The initial distribution was highly skewed with the median 3.15, but was normalised using an arctan tranformation, as used by Suwa et al. [116] for

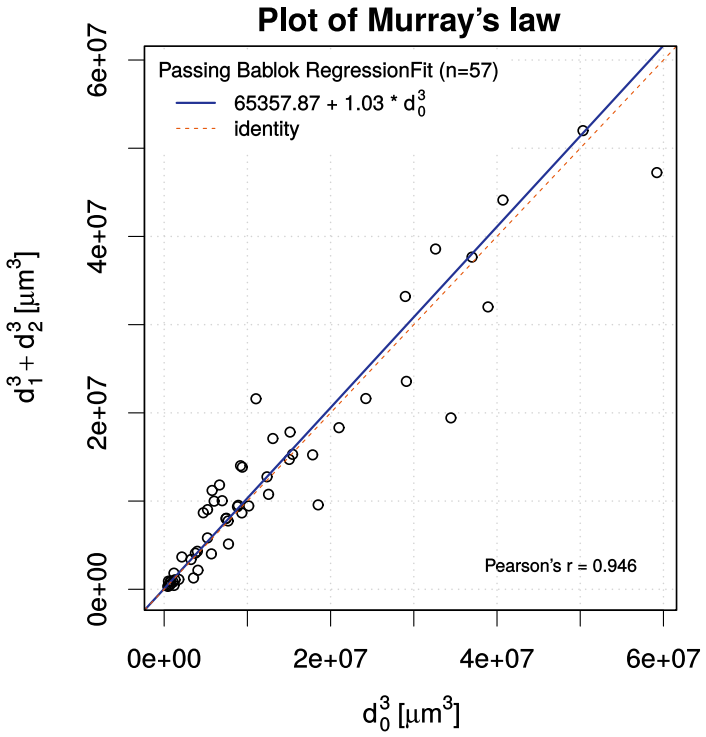

Fig. 4.10 Plot of $d_1^3 + d_2^3$ versus d_0^3. The blue solid line is a regression fit by Passing-Bablok method, and the red dashed line indicates the identical line.

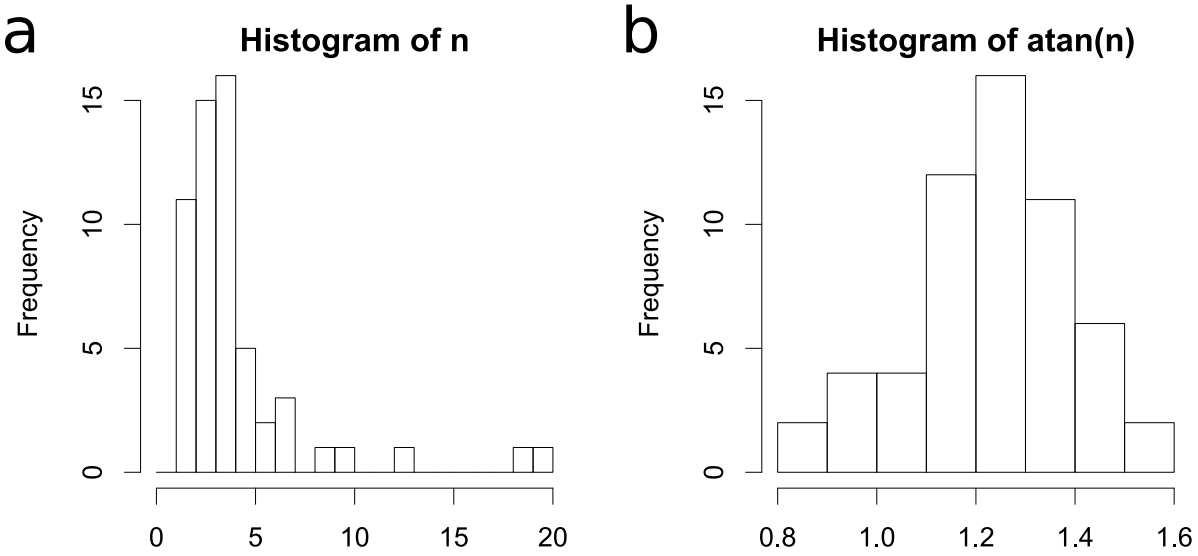

Fig. 4.11 (a) Histogram showing the distribution of the vessel scaling exponent n calculated from $d_0^n = d_1^n + d_2^n$ for all bifurcations in the set of circular evacuation networks. (b) The $\arctan(n)$ transformation normalised the data and gives a mean $\pm$ S.D. of 1.235 ± 0.045

blood vessel networks Fig. 4.11b. The correlation coefficient between $\arctan n$ and r_0 was 0.015 and the mean and 95% confidence interval were 1.235 ± 0.045. This gave an estimate of n from the tangent of the interval as between 2.53 to 3.29, which appears to be reasonably consistent with the expectation of $n \sim 3$ from Murray's law. Nevertheless, we do not have a good understanding of the extreme values of n in the measured distribution.

4.2.2 Relationship between branching angle and thickness ratio

According to Murray [16], when a vein ramifies into two veins with diameters d_1 and d_2, the angle φ between the daughter veins is predicted as

$$\varphi = \arccos \frac{(1+\beta^3)^{4/3} - 1 - \beta^4}{2\beta^2}, \tag{4.1}$$

where $\beta = d_1/d_2$. Note that φ takes the same value for $\beta = d_1/d_2$ and $\beta = d_2/d_1$. To verify this prediction, φ was measured for the 57 junctions and β was calculated so that $\beta \leq 1$. As shown in Fig. 4.12a, φ distributed around the predicted line but the variance was not so small.

Murray [16] also stated that for the branching angle φ_1 and φ_2,

$$\varphi_1 = \arccos \frac{1 + \alpha_1^4 - (1-\alpha_1^3)^{4/3}}{2\alpha_1^2}, \tag{4.2}$$

$$\varphi_2 = \arccos \frac{1 + \alpha_2^4 - (1-\alpha_2^3)^{4/3}}{2\alpha_2^2}, \tag{4.3}$$

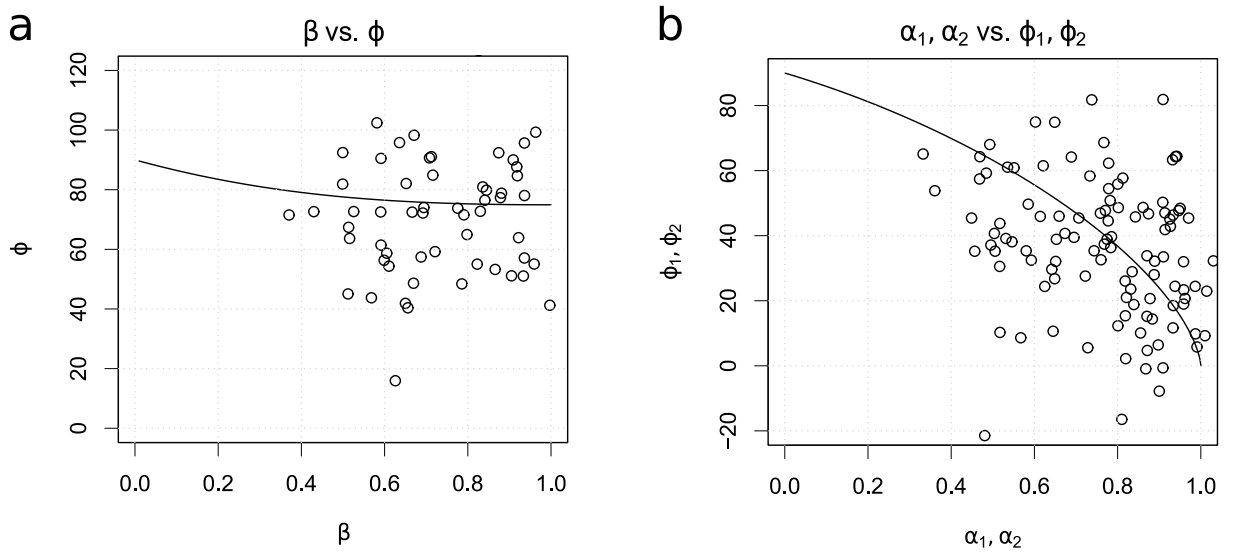

Fig. 4.12 Relationship between branching angle and thickness ratio. The solid lines of (a) indicate curves of Eq. (4.1), and that of (b) indicate Eq. (4.2) and Eq. (4.3).

where $\alpha_1 = d_1/d_0$ and $\alpha_2 = d_2/d_0$ are thickness ratios. For the 57 junctions, φ_1, φ_2, α_1, and α_2 were measured and calculated as shown in Fig. 4.12b, in which data points distributed around the prediction.

In both plots, Murray's curves fitted to the plots with large variance, which indicated that his theory was roughly correct but some assumptions were inappropriate. Speaking concretely, he considered minimization of total volume of arteries under a condition in which tubes connected fixed points, whereas in this experiment, the exit was fixed but other evacuation points were distributed in the arena and not assigned specifically. That is, degree of freedom on the points to be connected may cause fluctuations on his angle theory.

Chapter 5

Mathematical Modelling

5.1 Application of current-reinforcement to evacuating plasmodium

Now we apply current-reinforcement dynamics to the evacuation of plasmodium, which created vein network from an uniform state within migration through a narrow exit. For that purpose, appropreate implementation of experimental situation is necessary, that is, we need to set sources and sink. Whilst they are usually considered as food sources, there was only one food outside of the exit in the experimental environment, and only one source or sink does not satisfy the constraint of Eq. (2.29). However, we inferred from the results that plasmodium evacuated from arena equivalently, which implies uniform divergence of body mass in arena. Hence, we set

$$J(v) = \begin{cases} J_0, & v \text{ is not the exit,} \\ -(N-1)J_0, & v \text{ is the exit.} \end{cases} \tag{5.1}$$

Regarding the flow function $f(|Q_{ij}|)$, we set $f(|Q_{ij}|) = |Q_{ij}|^\mu$, where we call the parameter μ *flow exponent* as Tero *et al.* originally assumed [8]. Finally, as the initial state, we assumed random tubular meshwork with uniform very small radius, which meant no channels in arena.

Virtual arenas were constructed to match the shapes used in the experiment with a scale 10 μm/px, and a random mesh, generated by a Delaunay triangulation with random vertices giving density of 1/500 px^{-2} within the arena shape. A single vertex at the exit was designated as a sink, whilst all others were set as sources with $J_0 = 0.1$. The radii r of all veins were set to be 0.1 initially, and the conductivity was equal to r^4. Simulations were run on MATLAB with a short initial time step ($\Delta t = 0.001$) over the period $t = 0$ to $t = 0.1$, followed by $\Delta t = 0.01$ for $t = 0.11$ to $t = 1$, and $\Delta t = 0.1$ for $t = 1.1$ to $t = 50$ (see Appendix for the actual code). Note that we did not attempt to model the change in thickness of the rest of the plasmodial sheet, which might be represented as variation of the input current to each node over time, as the purpose of the simulation was to capture the initial development of the evacuation network.

5.2 Simulated evacuation network for various parameters and arena shapes

Fig. 5.1 shows the simulation results with flow exponents $\mu = 0.8, 1, 1.33, 2$ and 4 in the circular shape, where vein structure are changed gradually from the initial thin and uniform vein networks and reached a steady state as the time development. Similar time developments were obtained for other shapes as the results for $\mu = 1.33$ are shown in Fig. 5.2 and 5.3. The network morphology of the final state with flow exponents $\mu = 0.8, 1, 1.33, 2$ and 4 in different shapes are shown in Fig. 5.4.

When flow exponent was greater than 1, a subset of the available veins thickened and formed a branching tree from the exit site with progressively thinner veins through repetitive bifurcations towards the boundary of the arena. When flow exponent was 1, the branching tree contained additional loops, whilst when flow exponent was less than one, the vein thicknesses were more homogeneous and there were many loops. Visual inspection suggested that flow exponent to be 1.33 and 2 most closely resembled the experimental data.

5.3 Resemblance to real networks regarding space-filling property and diameter exponent

To compare the simulated networks quantitatively with the experimental network, the normalised Hausdorff distance was calculated for the main network, defined as the set of veins containing the top 10% of the thickest veins (Fig. 5.5). This limit was selected to contain the minimum radii in the simulation that could be measured in the experimental networks. Although it was unclear which veins are the main network for the case of $\mu \leq 1$ (Fig. 5.4), we applied this criteria for all results, so that some main networks of $\mu \leq 1$ are fragmented and concentrated near the exit. The calculated normalised Hausdorff distance was small across all arena shapes, and similar to the values observed for the experimental systems, particularly for $\mu > 1$ (Fig. 5.6). We infer that the current-reinforcement simulation model can reproduce the basic characteristics of the experimental *Physarum* networks when flow exponent μ is greater than 1.

In addition to the analysis of Hausdorff distance, we estimated diameter exponent for each flow exponent from main veins. In Fig. 5.7, diameter exponents calculated for each three-way junction of main veins of the simulation are plotted, giving 95% confidence intervals $[0.96, 0.97]$, $[1.93, 1.95]$, $[2.90, 2.93]$, $[4.04, 4.14]$, and $[6.12, 6.51]$ for flow exponents 0.8, 1, 1.33, 2, and 4, respectively. Thus, the flow exponent $\mu = 1.33$ is very good correspondece to the result of experiment which shows diameter exponent $n = 3$, that is, Murray's law.

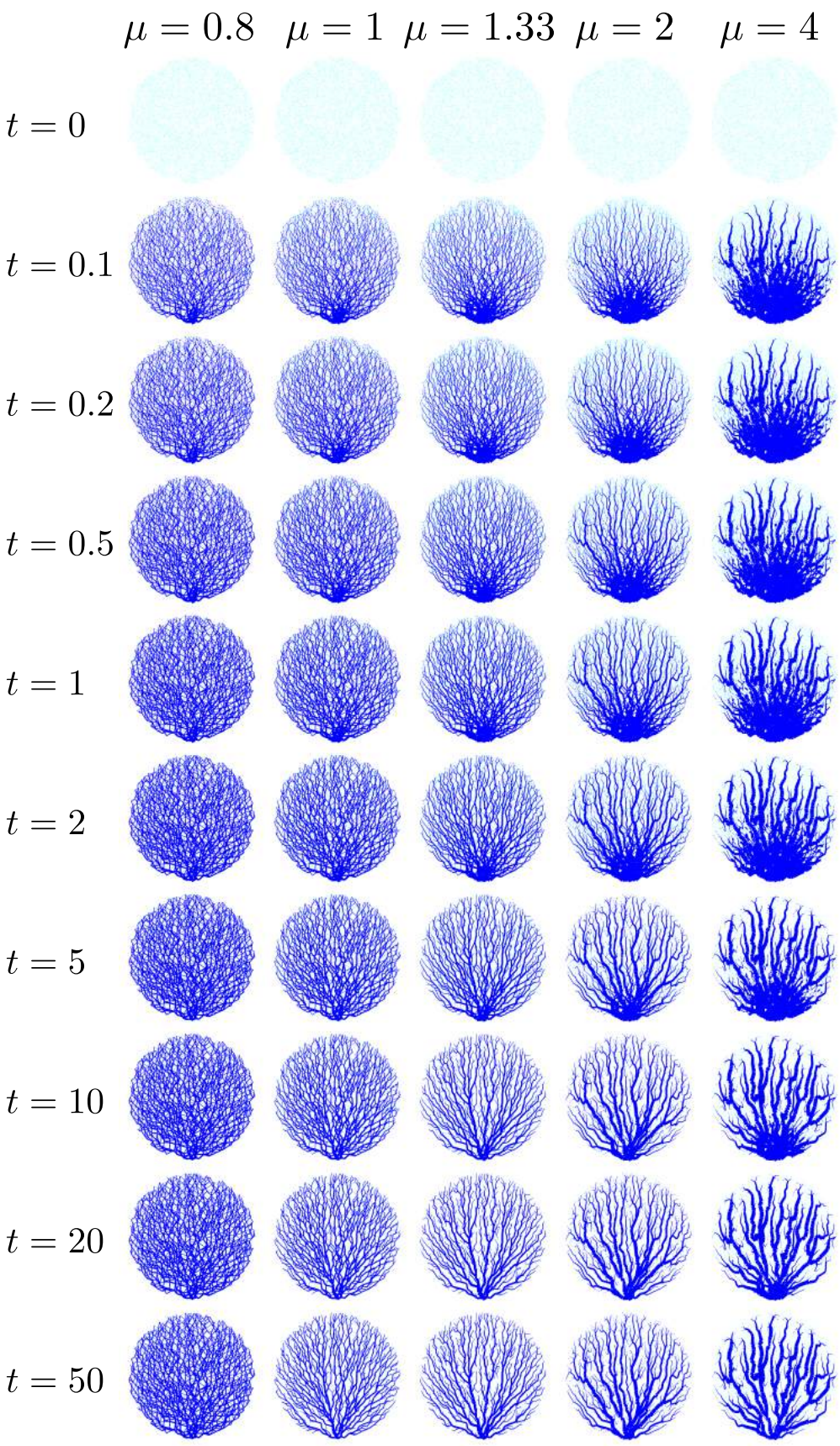

Fig. 5.1 Simulation results for varying flow exponent μ in the circular shape. The main veins are drawn in proportion to the simulation result with the common limitation of maximum radius, whilst the very thin veins are drawn with dashed, dotted, or light blue line.

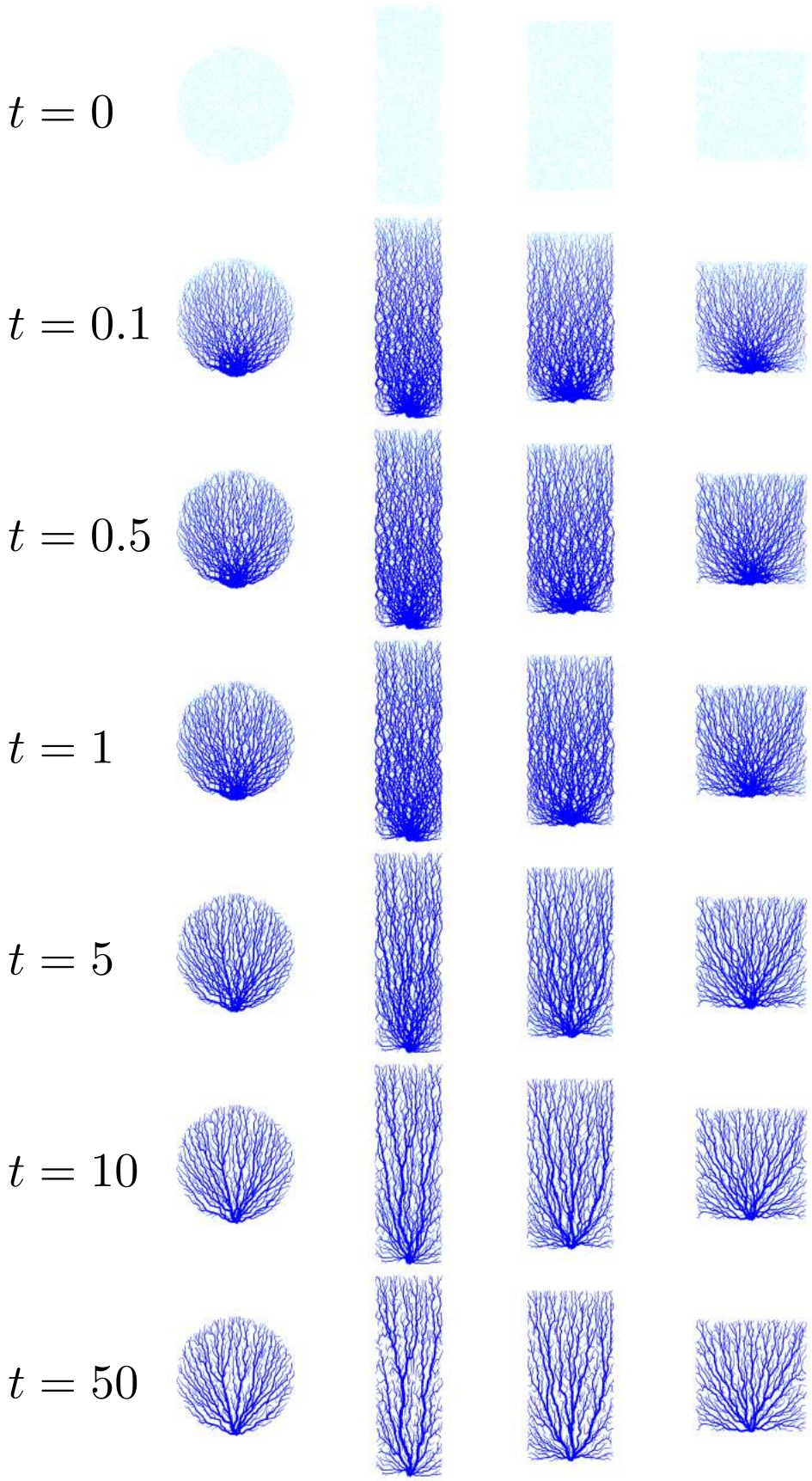

Fig. 5.2 Simulation results in the different arena shapes (C, R1, R2, and R3, from left) for flow exponent $\mu = 1.33$. The veins are drawn in the same way to Fig. 5.1

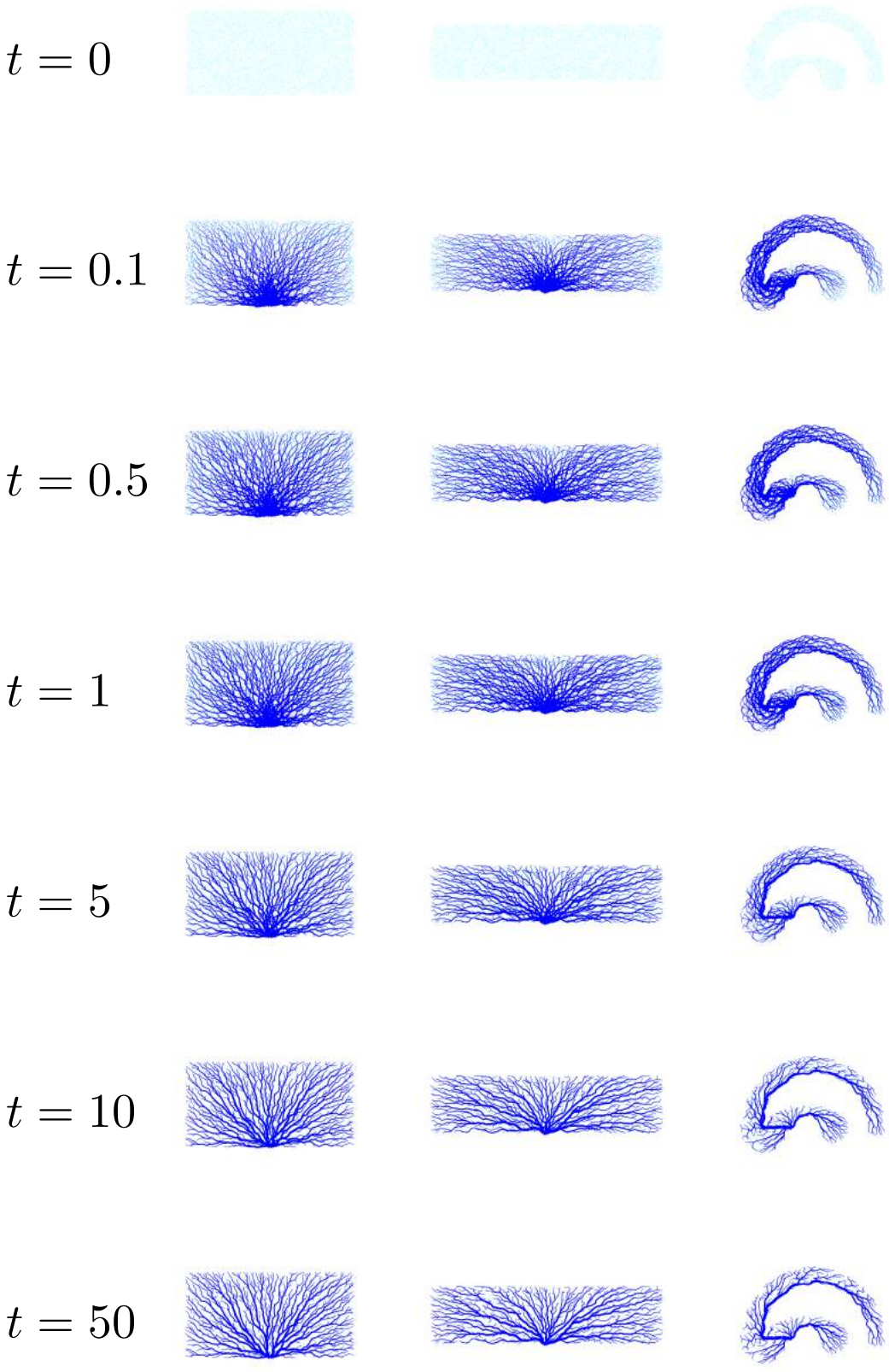

Fig. 5.3 Simulation results in the different arena shapes (R4, R5, and A, from left) for flow exponent $\mu = 1.33$. The veins are drawn in the same way to Fig. 5.1

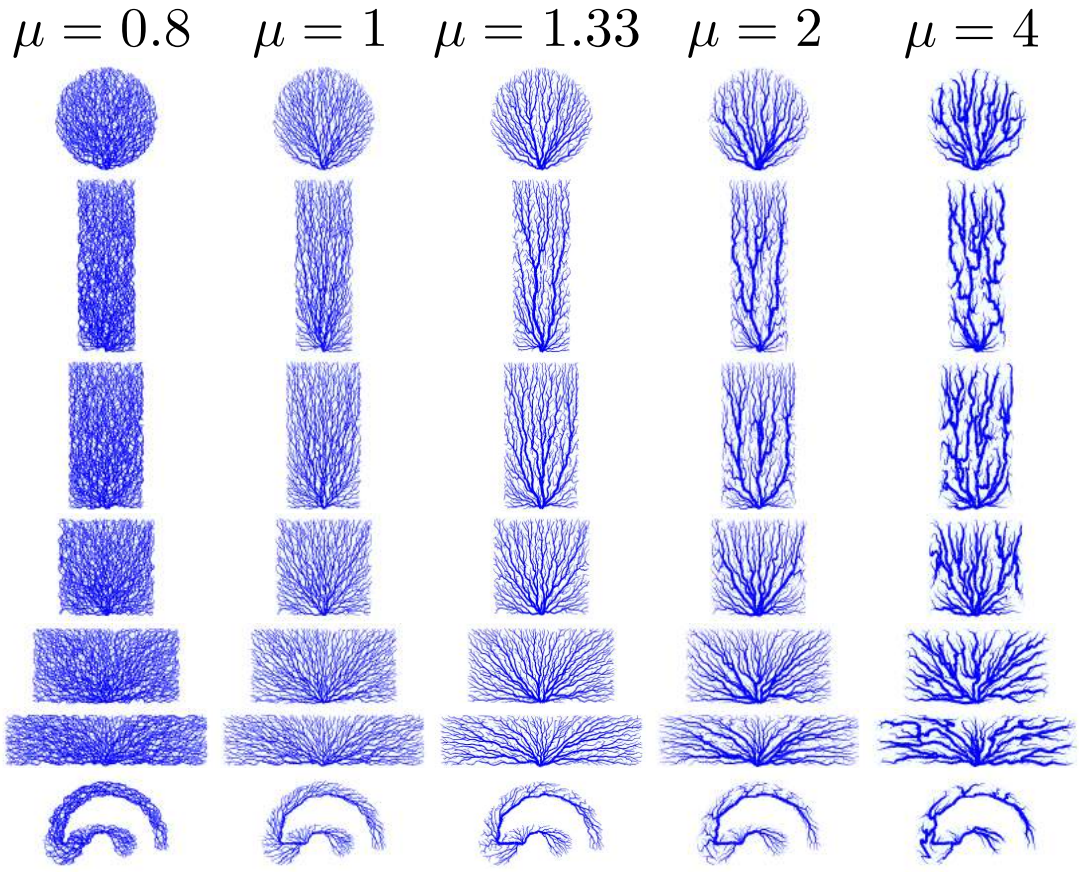

Fig. 5.4 The final states of simulations for varying flow exponent μ in the different arena shapes (C, R1, R2, R3, R4, R5, and A, from top). The veins are drawn in the same way to Fig. 5.1

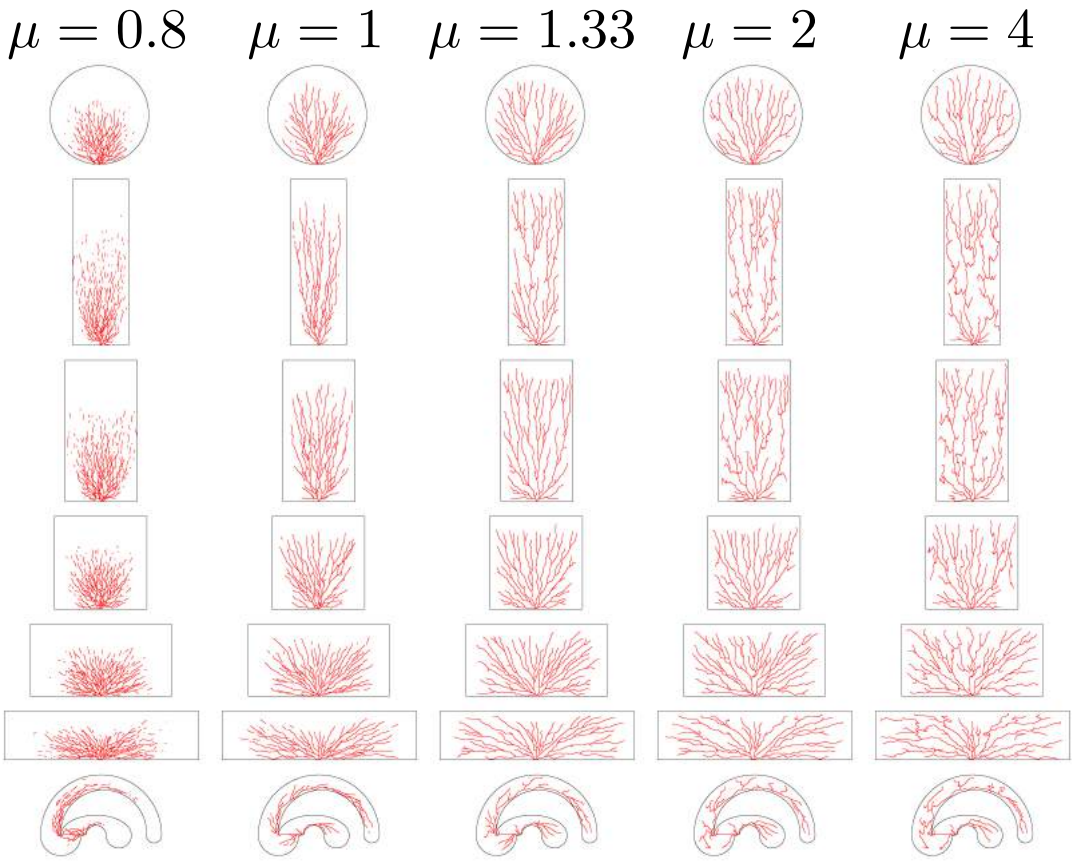

Fig. 5.5 Main networks from the simulation model, defined as the top 10% of the thickest veins.

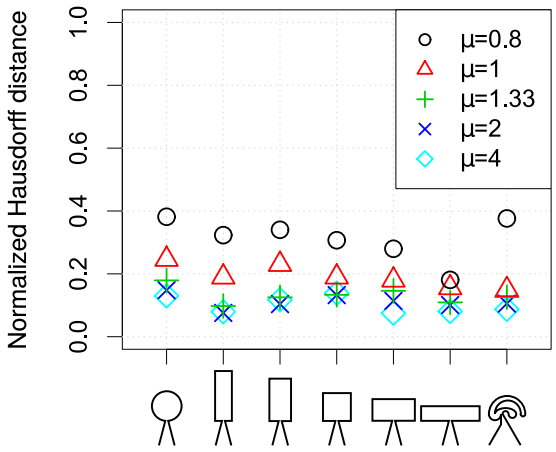

Fig. 5.6 Normalized Hausdorff distance between the simulated main network and all points in the arena.

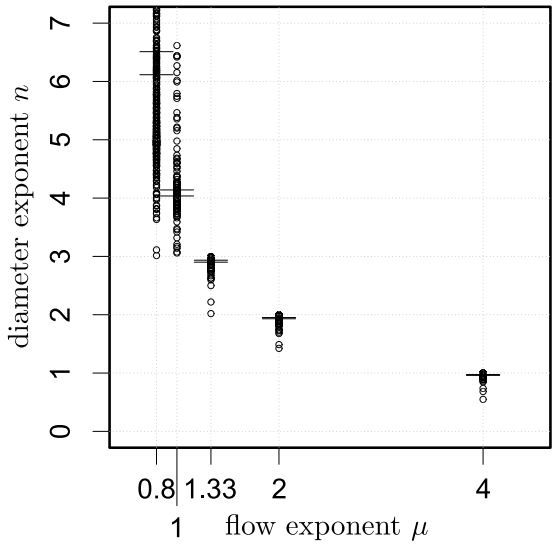

Fig. 5.7 Diameter exponents of triple junction in main veins of simulation plotted against flow exponents.

5.4 Impact of flow exponent on network volume and viscous drag

Murray's theory [16], in which balance of the energy required to overcome viscous drag forces and the cost of maintaining the volume of the network, achieved one of geometric laws of biological transport network. It is therefore instructive to examine the time-evolution of these two parameters and their dependence on μ in the simulation model as the system tends towards steady-state.

The change in the energy required for transport over time for simulations of the circular arena is shown in Fig. 5.8 (the initial change is magnified in Fig. 5.9), where the total frictional energy was calculated as:

$$E = \sum_{i \in \text{veins}} \Delta P_i Q_i = \sum_{i \in \text{veins}} \frac{L_i Q_i^2}{D_i}. \tag{5.2}$$

During the initial stages of the simulation the frictional energy decreased rapidly as the network shifted from the random network of tubes with homogeneous low diameter, to the branching tree morphology (Fig. 5.9, top). The minimum energy dissipation was achieved with $\mu = 4/2$. Nevertheless, the time course was not quite monotonic, with a slow increase observed after the minimum value was reached around t=2.5 (Fig. 5.8, top), consistent with the contribution of other factors in the cost function.

The total volume of the tubular veins, representing the energy cost to maintain the network [16], was calculated as:

$$V = \sum_{i \in \text{veins}} \frac{\pi r_i^2 L_i}{2}, \tag{5.3}$$

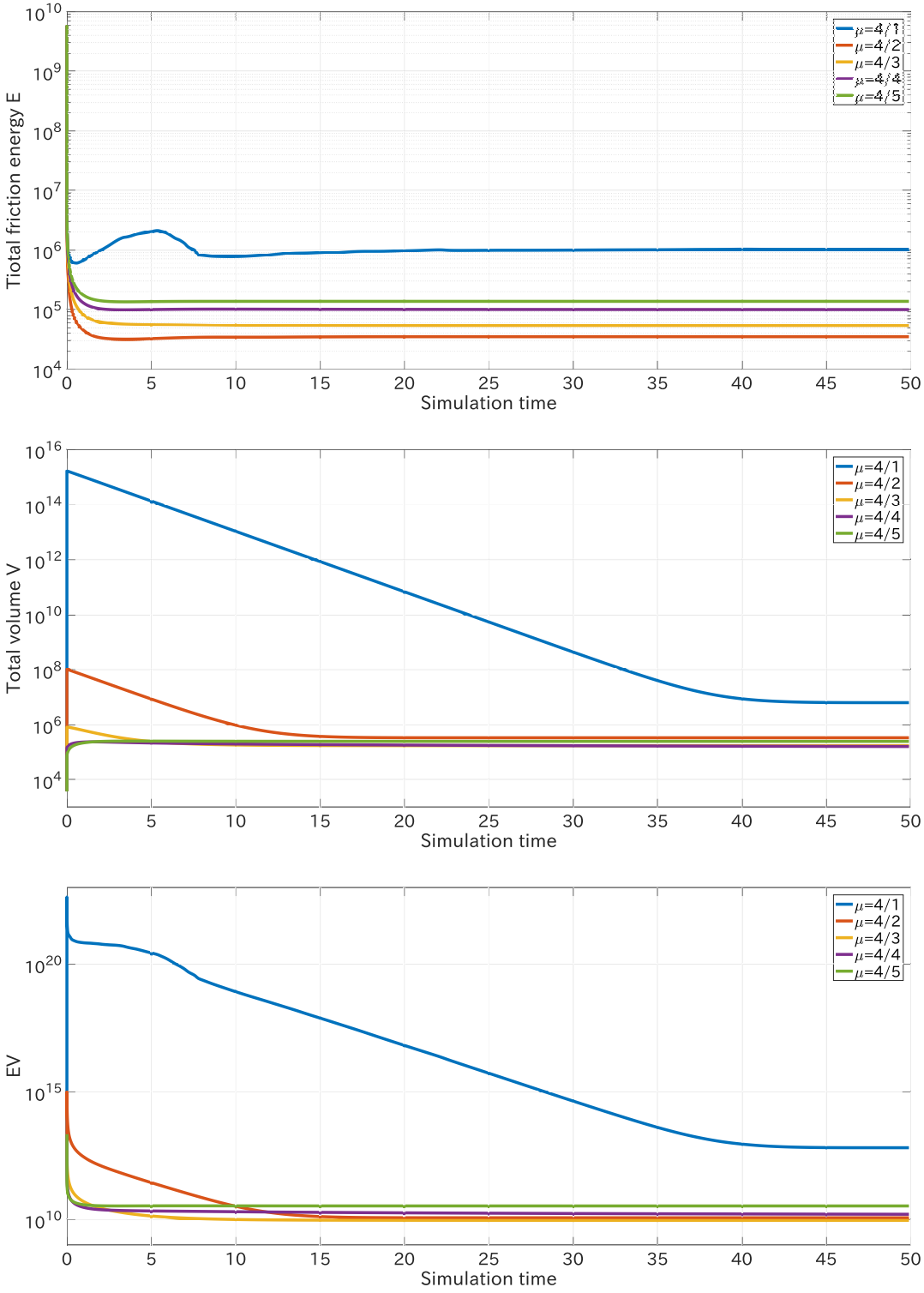

Fig. 5.8 Time courses for the change in frictional energy E (top), total volume V (middle), and their product EV (bottom) for the simulation results from the circlular arena.

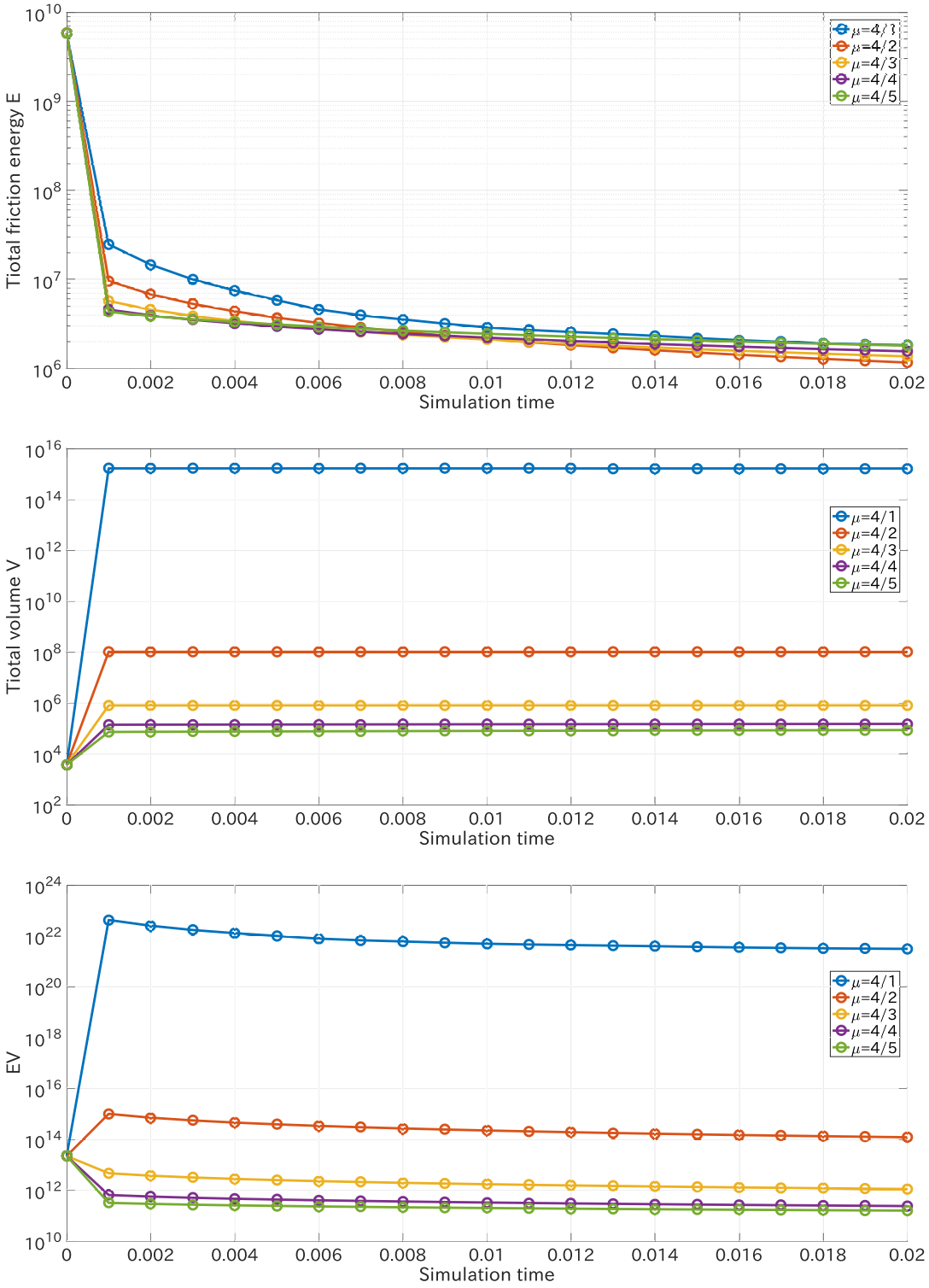

Fig. 5.9 Initial changes of frictional energy E (top), total volume V (middle), and their product EV (bottom) for the simulation results from the circular arena.

The total volume of the network increased in the very early phase of the numerical simulation, particularly in the case of $\mu \leq 4/3$ (Fig. 5.9, middle). This pronounced surge was caused by setting the initial tube radii to be small (0.1) and equal to mimic the emergence of the tubular network from a uniform sheet. The total volume of the network then gradually declined to a steady state value by the end of the simulation (Fig. 5.8, middle). In the steady state, the lowest network volume was realised with $\mu = 4/4$, almost same value with $\mu = 4/3$ (Fig. 5.8, middle).

Following expectations from Murray's Law, we examined the combination ($E \times V$) of the friction energy and the total volume (see Fig. 5.8, bottom). The steady state value of $E \times V$ was the lowest for $\mu = 4/3$, and the minimum was realized in a relatively early phase of time course.

Taken together, it appears that (i) self-organised network formation in *Physarum* conforms to a scaling coefficient of $\mu = 4/3$ in experimental results; (ii) when the same 4/3 scaling is used in the biologically-inspired current-reinforcement model, it simulates the overall characteristics of the real network; and (iii) the model minimises the combination of network volume and frictional energy.

Chapter 6

Conclusions and Discussions

6.1 Evacuation transport network

6.1.1 Adaptive network formation of *Physarum polycephalum*

It is less clear how the network forms from an initially homogeneous plasmodial sheet. It is known that actin-myosin interactions generate contractions in small plasmodial droplets that can become organised as propagating waves or spirals (e.g. [120]). This provides a driving force for protoplasmic streaming, although initially it is undirected and uniform across the plasmodium. However, Guy *et al.* proposed for a migrating plasmodium that an initially homogeneous flow of protoplasmic sol can de-stabilise the actin skeleton as it moves through the porous protoplasmic gel [121]. This in turn initiates channel formation if the flow is sufficiently rapid, through flow-dependent actin disruption and gel-sol interconversion. Such a process appears to operate rapidly in the newly formed plasmodium, as the emergent network spanning the entire arena is visible with a few hours, correctly oriented towards the exit, and remains stable until the arena is almost fully evacuated (Fig. 4.1).

6.1.2 Biological significance of homogeneous evacuation

From its inception, the network is able to drain all parts of the arena equally irrespective of the shape. From a biological perspective the plasmodium in the arena has no access to food, so it makes sense to re-deploy the biomass elsewhere as rapidly as possible. Equally, it is important that the exit does not becomes clogged nor should the plasmodium become disconnected, prioritising an orderly evacuation sequence. In the case of *Physarum* this appears to emerge as a natural consequence of the current-reinforcement model that establishes a similar hydrodynamic conductivity from all peripheral parts of the network. This is in stark contrast to observations and models of human evacuation, where exit routes rapidly become jammed with rushing people, and further movement is restricted by the strong frictional force between trapped pedestrians [122], although exit rates can be improved by placing an obstacle off-center and just in front of the exit [123].

6.1.3 Bottleneck as a information hub

In the evacuation experiment conducted here, the exit acts as a bottleneck that controls protoplasmic redeployment as all the biomass must pass through this point. As the rate of draining is homogeneous across the arena, the contribution of biomass from every local part of the plasmodial sheet to the bottleneck is equal. Nevertheless, on the timescale of minutes, shuttle streaming of protoplasm rapidly mixes the cytoplasm within the plasmodium [15], with biomass periodically transported both to the bottleneck and back to the periphery. Interestingly, this means that both biophysical changes, such as mechanical momentum of mass flow, and chemical components, such as nutrients or signalling molecules, may cycle between distal parts of the plasmodium and the bottleneck. This opens the possibility for information transfer of either physical or chemical signals to and from the bottleneck, which acts as a transient hub controlling intracellular communication through the vein network. Such organization of network structure may be required to co-ordinate behaviour in response to local information that could be sensed at any part of the plasmodium. In other words, all local regions are homogeneously inspected by the bottleneck at regular intervals. This implies that the plasmodium has the potential ability to organize an *ad hoc* functional center in response to varying external conditions.

6.2 Current-reinforcement as a tubular development dynamics

6.2.1 Relationship between the parameter and diameter exponent

The plasmodium of the slime mold *Physarum polycephalum* spontaneously creates complex networks that provide an accessible model for the development of self-organised adaptive transport systems. It is capable of solving path-finding problems [10, 11], and can realise reasonable solutions to complex spatial network tasks designed to mimic human infrastructure networks. For example, Tero *et al.* [9] showed that the vein network constructed by *Physarum* on agar constrained to the Kanto region of Japan was comparable to the real JR railway network in terms of transport efficiency and resilience. In a similar manner, Adamatzky and Jones have compared road networks in the UK, USA, and Germany with those made by *Physarum* [93, 94]. In parallel, a number of models have emerged that capture the behaviour of *Physarum* using current-reinforcement rules where the flow modifies the network architecture, which in turn modifies the flows. Nevertheless, the models have not so far been parametrised directly from the experimental data, nor have the functional form of the feedback terms been linked to theoretical expectations from fluid flow dynamics.

Actually, we can infer linkage between experimental results and current-reinforcement dynamics. Considering the equilibrium state of the model as $\mathrm{d}D_{ij}/\mathrm{d}t = 0$, we see that

$$|Q_{ij}|^{\mu} = D_{ij} \propto r_{ij}^{4}, \tag{6.1}$$

which means $|Q_{ij}| \propto r_{ij}^{4/\mu}$. Therefore, using the notation of 4.2.1, we can express the

exponent rule as

$$r_0^{4/\mu} = r_1^{4/\mu} + r_2^{4/\mu} \tag{6.2}$$

and see the correspondence to the diameter exponent $n = 4/\mu$, which means Murray's law holds in a steady state of the model with $\mu = 4/3$. Thus in this paper, we have first measured the development of an evacuation network as *Physarum* exits a bounded arena to determine whether the network geometry follows expectations from fluid dynamics and energy minimisation criteria developed by Murray [16], and second examined the consequence of running the current-reinforcement model with the experimentally-validated 4/3 scaling coefficient.

The results provide evidence that *Physarum* does obays Murray's law, which implies the cost balance behaviour, and that simulations run with this parameter provide comparable solutions, whilst minimising the combination of shear stress and vessel volume. It is possible that the fit to the data could be improved with more precise measurement of the actual cross-sectional area available for flow within the tube, rather than our manual estimate from the external tube diameter, assuming there is an almost linear relationship between internal and external diameter [124]. Nevertheless, to our knowledge, this is the first time that experimental network formation, network theory and network simulation have all converged to give consistent results in a model system.

6.2.2 Shear stress: a factor of vein development

Interestingly, as the *Physarum* network appears to follow the exponent scaling predicted by Murray's Law, we can also make predictions concerning the wall shear stress throughout the network. The shear stress $\tau(r)$ at the wall caused by Hagen-Poiseuille flow in a cylindrical tube (radius r_0) is given by

$$\tau(r) = -\eta \left.\frac{\partial v(x)}{\partial x}\right|_{x=r} = -\frac{r_0}{2}\frac{\Delta P}{L} \tag{6.3}$$

from the velocity profile of Eq. (2.25). Substituting $Q = (\pi r_0^4/8\eta)(\Delta P/L)$ into the above shear stress formula, we obtain

$$Q = \frac{\tau(r)\pi r^3}{4\eta}. \tag{6.4}$$

Combining this and the mass conservation around the bifurcation point of vein $Q_0 = Q_1 + Q_2$, we find

$$\tau(r_0)r_0^3 = \tau(r_1)r_1^3 + \tau(r_2)r_2^3 \tag{6.5}$$

where r_0, r_1, and r_2 are radii of parent vein and two daughter veins, respectively.

As the experimental results confirm $r_0^3 = r_1^3 + r_2^3$, we infer that $\tau(r_0)$, $\tau(r_1)$ and $\tau(r_2)$ are equal to satisfy Eq. (6.5), meaning that the shear stress is equal in all veins irrespective of their thickness. This also suggests that the average velocity $\bar{v}$ is proportional to r_0 because

$$Q = -\pi r^2 \bar{v} = \frac{\pi \tau r^3}{4\eta}, \tag{6.6}$$

which means

$$\bar{v} = \frac{\tau}{4\eta} r. \tag{6.7}$$

This relationshiop is supported by some studies of Takamatsu *et al.* [124, 125], where velocities increased linearly with width for tubes constrained in a narrow channels. Whilst the molecular mechanism underpinning current-reinforcement is not known yet, this observation leads to the interesting possibility that sensing an increase in wall shear above a fixed point provides a molecular trigger to changing vessel diameter. Thick bundles of actin filament are observed to co-align with each other at the interface between the vein wall and the flowing fluid along these emerging channels as they thicken to become veins [126]. Shear stress at the vein wall is a good candidate to align the F-actin bundles, in a similar manner to that reported for shear banding of F-actin in solution [127]. Interistingly, Kamiya and Togawa [128] found an adaptive regulation in canine carotid artery, in which thickness was adjusted with flow and shear stress was maintained in constant. These facts indicate the importance of shear forces in the control of vessel development in organisms.

6.2.3 Further improvement on current-reinforcement model

The current-reinforcement model generated networks similar to those found experimentally, although the kinetics leading to emergence of the network in the model differed, particularly in the early stages, where the initial conditions dominated behaviour of the simulation. For example, starting with uniform small radii and constant input current to find the initial flow in each vein also required extremely high pressures in the peripheral part of the arena, with consequential increases in friction energy and total volume (Fig. 5.8), until some tubes with larger diameter emerged. In addition, the simulation model did not predict the long-term evacuation dynamics as the current input rate to each node did not decrease as would be expected as the mass was evacuated.

The principles of current-reinforcement are well-established for a number of biological systems as diverse as ant trails and human trails [14]. The precise form of the model is context specific, but most models incorporate similar elements. For example, Hu and Cai [4] proposed a very similar model which is, in our notation, expressed as

$$\frac{\mathrm{d}D_{ij}}{\mathrm{d}t} = c\left(\frac{Q_{ij}^2}{D_{ij}^{\gamma+1}} - \tau_e^2\right) D_{ij}, \tag{6.8}$$

where c, γ, and τ_e are constants. Furthermore, Haskovec *et al.* [129, 130] presented a system of partial differential equations that contained a current term effecting a time evolution of conductivity. While these models consider specific current effects, the model of Eq. (2.31) can take an arbitrary thickening factor $f(|Q_{ij}|)$. There is increasing interest in exploring the limits of behaviour for generic current-reinforcement dynamics and how these may play out on network topologies other than 2-D planar systems where they first emerged, where they show very rich behaviour (e.g., [131]).

Acknowledgement

I gratefully appreciate instructions and supports of Prof. Toshiyuki Nakagaki, Associate Prof. Katsuhiko Sato, Assistant Prof. Shigeru Kuroda. I would also like to express my appreciation to Dr. Itsuki Kunita, Kumamoto University, Associate Prof. Mark Fricker, University of Oxford, Associate Prof. Kei-ichi Ueda, University of Toyama, Assistant Prof. Kentaro Ito, Hiroshima University, Associate Prof. Yuka Yajima, Muroran Institute of Technology, and Prof. Hisashi Haga, Hokkaido University. For the supports on my doctor course, I would like to thank Associate Prof. Akimasa Fukui, Associate Prof. Tomoyasu Aizawa, and staffs of Graduate School of Life Science. I owe my school life to the scholorship of Morishita Jintan and the loan of Japan Student Services Organization. I deeply appreciate the financial supports. In addition, I appreciate all the taxpayers in Japan as a student of a national university. I also thanks to all lab members, friends, and my family.

Bibliography

[1] G. B. West, J. H. Brown and B. J. Enquist, "A general model for the origin of allometric scaling laws in biology", Science, **276**, 5309, pp. 122–126 (1997).

[2] J. R. Banavar, A. Maritan and A. Rinaldo, "Size and form in efficient transportation networks", Nature, **399**, 6732, pp. 130–132 (1999).

[3] P. S. Dodds, "Optimal form of branching supply and collection networks", Phys. Rev. Lett., **104**, p. 048702 (2010).

[4] D. Hu and D. Cai, "Adaptation and optimization of biological transport networks", Phys. Rev. Lett., **111**, p. 138701 (2013).

[5] F. Corson, "Fluctuations and redundancy in optimal transport networks", Phys. Rev. Lett., **104**, p. 048703 (2010).

[6] E. Katifori, G. J. Szöllősi and M. O. Magnasco, "Damage and fluctuations induce loops in optimal transport networks", Phys. Rev. Lett., **104**, p. 048704 (2010).

[7] T. Nakagaki, H. Yamada and T. Ueda, "Interaction between cell shape and contraction pattern in the physarum plasmodium", Biophysical Chemistry, **84**, 3, pp. 195 – 204 (2000).

[8] A. Tero, R. Kobayashi and T. Nakagaki, "A mathematical model for adaptive transport network in path finding by true slime mold", Journal of Theoretical Biology, **244**, 4, pp. 553 – 564 (2007).

[9] A. Tero, S. Takagi, T. Saigusa, K. Ito, D. P. Bebber, M. D. Fricker, K. Yumiki, R. Kobayashi and T. Nakagaki, "Rules for biologically inspired adaptive network design", Science, **327**, 5964, pp. 439–442 (2010).

[10] T. Nakagaki, M. Iima, T. Ueda, Y. Nishiura, T. Saigusa, A. Tero, R. Kobayashi and K. Showalter, "Minimum-risk path finding by an adaptive amoebal network", Phys. Rev. Lett., **99**, p. 068104 (2007).

[11] T. Nakagaki, H. Yamada and Á. Tóth, "Intelligence: Maze-solving by an amoeboid organism", Nature, **407**, 6803, pp. 470–470 (2000).

[12] W. Baumgarten, T. Ueda and M. J. Hauser, "Plasmodial vein networks of the slime mold physarum polycephalum form regular graphs", Physical Review E, **82**, 4, p. 046113 (2010).

[13] A. Fessel, C. Oettmeier, E. Bernitt, N. C. Gauthier and H.-G. Döbereiner, "*Physarum polycephalum* percolation as a paradigm for topological phase transitions in transportation networks", Phys. Rev. Lett., **109**, p. 078103 (2012).

[14] Q. Ma, A. Johansson, A. Tero, T. Nakagaki and D. J. T. Sumpter, "Current-reinforced random walks for constructing transport networks", Journal of The Royal Society Interface, **10**, 80 (2012).

[15] K. Alim, G. Amselem, F. Peaudecerf, M. P. Brenner and A. Pringle, "Random network peristalsis in physarum polycephalum organizes fluid flows across an indi-

vidual", Proceedings of the National Academy of Sciences, **110**, 33, pp. 13306–13311 (2013).

[16] C. D. Murray, "The physiological principle of minimum work applied to the angle of branching of arteries", The Journal of General Physiology, **9**, 6, pp. 835–841 (1926).

[17] T. F. Sherman, "On connecting large vessels to small. the meaning of murray's law.", The Journal of General Physiology, **78**, 4, pp. 431–453 (1981).

[18] C. A. Price, J. S. Weitz, V. M. Savage, J. Stegen, A. Clarke, D. A. Coomes, P. S. Dodds, R. S. Etienne, A. J. Kerkhoff, K. McCulloh, K. J. Niklas, H. Olff and N. G. Swenson, "Testing the metabolic theory of ecology", Ecology Letters, **15**, 12, pp. 1465–1474 (2012).

[19] M. G. Newberry, D. B. Ennis and V. M. Savage, "Testing foundations of biological scaling theory using automated measurements of vascular networks", PLoS Comput Biol, **11**, 8, pp. 1–18 (2015).

[20] V. Teplov, Y. Romanovsky and O. Latushkin, "A continuum model of contraction waves and protoplasm streaming in strands of physarum plasmodium", Biosystems, **24**, 4, pp. 269 – 289 (1991).

[21] M. Radszuweit, H. Engel and M. Bär, "A model for oscillations and pattern formation in protoplasmic droplets of physarum polycephalum", The European Physical Journal Special Topics, **191**, 1, pp. 159–172 (2010).

[22] K.-i. Ueda, S. Takagi, Y. Nishiura and T. Nakagaki, "Mathematical model for contemplative amoeboid locomotion", Physical Review E, **83**, 2, p. 021916 (2011).

[23] M. Radszuweit, S. Alonso, H. Engel and M. Bär, "Intracellular mechanochemical waves in an active poroelastic model", Phys. Rev. Lett., **110**, p. 138102 (2013).

[24] M. Radszuweit, H. Engel and M. Bär, "An active poroelastic model for mechanochemical patterns in protoplasmic droplets of *Physarum polycephalum*", PLoS ONE, **9**, 6, pp. 1–12 (2014).

[25] S. Alonso, U. Strachauer, M. Radszuweit, M. Bär and M. J. Hauser, "Oscillations and uniaxial mechanochemical waves in a model of an active poroelastic medium: Application to deformation patterns in protoplasmic droplets of physarum polycephalum", Physica D: Nonlinear Phenomena, **318319**, pp. 58 – 69 (2016).

[26] O. L. Lewis, S. Zhang, R. D. Guy and J. C. del Álamo, "Coordination of contractility, adhesion and flow in migrating physarum amoebae", Journal of The Royal Society Interface, **12**, 106 (2015).

[27] J. Hutton, "Theory of the earth; or an investigation of the laws observable in the composition, dissolution, and restoration of land upon the globe", Transactions of the Royal Society of Edinburgh, **1**, pp. 209–304 (1788).

[28] J. Hutton, "Theory of the earth: With proofs and illustrations", Edinburgh (1795).

[29] G. W. White, "Playfair's Illustrations of the Huttonian Theory of the Earth", University of Illinois Press (1956).

[30] W. D. Thornbury, "Principles of Geomorphology", John Wiley & Sons Inc, 2nd ed. (1969).

[31] R. E. Horton, "Erosional development of streams and their drainage basins; hydrophysical approach to quantitative morphology", Geological Society of America Bulletin, **56**, 3, pp. 275–370 (1945).

[32] L. M. Brush, "Drainage basins, channels, and flow characteristics of selected sstream

in central pennsylvania", United States Geological Survey Professional Paper, 282-F (1961).
[33] L. B. Leopold and J. P. Miller, "Ephemeral streams: hydraulic factors and their relation to the drainage net", United States Geological Survey Professional Paper, 282-A (1956).
[34] N. D. Gordon, T. A. McMahon, B. L. Finlayson, C. J. Gippel and R. J. Nathan, "Stream Hydrology: An Introduction for Ecologists", 2nd ed. (2004).
[35] 高山茂美, "復刊 河川地形", 共立出版, 復刊 (2013).
[36] A. N. Strahler, "Hypsometric (area-altitude) analysis of erosional topography", Geological Society of America Bulletin, **63**, 11, pp. 1117–1142 (1952).
[37] M. A. Melton, "An analysis of the relations among elements of climate, surface properties, and geomorphology", Office of Naval Research Project NR 389-042, Technical Report No. 11 (1957).
[38] M. E. Morisawa, "Quantitative geomorphology of some watersheds in the appalachian plateau", Geological Society of America Bulletin, **73**, 9, pp. 1025–1046 (1962).
[39] S. A. Schumm, "Evolution of drainage systems and slopes in badlands at perth amboy, new jersey", Geological Society of America Bulletin, **67**, 5, pp. 597–646 (1956).
[40] R. L. Shreve, "Statistical law of stream numbers", Journal of Geology, **74**, pp. 17–37 (1966).
[41] R. L. Shreve, "Variation of mainstream length with basin area in river networks", Water Resources Research, **10**, 6, pp. 1167–1177 (1974).
[42] J. W. Kirchner, "Statistical inevitability of horton's laws and the apparent randomness of stream channel networks", Geology, **21**, 7, pp. 591–594 (1993).
[43] I. Rodríguez-Iturbe and A. Rinaldo, "Fractal River Basins: Chance and Self-Organization", Cambridge University Press, Reprint (2001).
[44] T. Bryndal, "The river systems in small catchments in the context of the horton ' s and schumm ' s laws–implication for hydrological modelling. the case study of the polish carpathians", Quaestiones Geographicae, **34**, 1, pp. 85–98 (2015).
[45] M. M. Key, P. N. W. Jackson and L. J. Vitiello, "Stream channel network analysis applied to colony-wide feeding structures in a permian bryozoan from greenland", Paleobiology, **37**, 02, pp. 287–302 (2011).
[46] B. Herlihy and N. K. Maebius, "The Human Body in Health and Illness", Saunders, 2nd ed. (2003).
[47] B. B. Mandelbrot, "The Fractal Geometry of Nature", W. H. Freeman and Company, 1st (1983).
[48] J. P. Richter, "The notebooks of leonardo da vinci", `https://en.wikisource.org/wiki/The_Notebooks_of_Leonardo_Da_Vinci`.
[49] R. F. Spaide, "Optical coherence tomography angiography signs of vascular abnormalization with antiangiogenic therapy for choroidal neovascularization", American Journal of Ophthalmology, **160**, 1, pp. 6 – 16 (2015).
[50] C. D. Murray, "A relationship between circumference and weight in trees and its bearing on branching angles", The Journal of General Physiology, **10**, 5, pp. 725–729 (1927).
[51] C. D. Murray, "The physiological principle of minimum work: I. the vascular system

and the cost of blood volume", Proceedings of the National Academy of Sciences of the United States of America, **12**, 3, pp. 207–214 (1926).
[52] 日野幹雄, "明解水理学", 丸善 (1983).
[53] 神谷瞭, 戸川達男, "血管分岐系の最適構造について", 生物物理, **13**, 2, pp. 76–81 (1973).
[54] A. Kamiya, T. Togawa and A. Yamamoto, "Theoretical relationship between the optimal models of the vascular tree", Bulletin of Mathematical Biology, **36**, pp. 311 – 323 (1974).
[55] 戸川達男, "血管の分岐の形態とその構築", 物性研究, **36**, 1, pp. A40–A47 (1981).
[56] H. Kitaoka, R. Takaki and B. Suki, "A three-dimensional model of the human airway tree", Journal of Applied Physiology, **87**, 6, pp. 2207–2217 (1999).
[57] K. Schmidt-Nielsen, "Scaling : why is animal size so important?", Cambridge University Press (1984).
[58] R. H. Peters, "The ecological implications of body size", Cambridge University Press (1983).
[59] M. Kleiber, "Body size and metabolism", Hilgardia, **6**, 11, pp. 315–353 (1932).
[60] A. Bejan, "The tree of convective heat streams: its thermal insulation function and the predicted 3/4-power relation between body heat loss and body size", International Journal of Heat and Mass Transfer, **44**, 4, pp. 699–704 (2001).
[61] G. C. Ainsworth, "Introduction to the History of Mycology", Cambridge University Press (1976).
[62] 山本幸憲, "図説 日本の変形菌", 東洋書林 (1998).
[63] 南方熊楠, "本邦産粘菌類目録", 植物学雑誌, **22**, 260, pp. 317–323 (1908).
[64] G. Lister, "Japanese mycetozoa", Transactions of the British Mycological Society, **5**, pp. 67–84 (1914).
[65] C. J. Alexopoulos and C. W. Mims, "Introductory mycology", John Wiley and Sons, 3rd ed. (1979).
[66] G. Lister, "New or rare species of mycetozoa", Journal of Botany, British and Foreign, **59**, pp. 89–93 (1921).
[67] 平野威馬雄, "大博物学者 - 南方熊楠の生涯", リブロポート (1982).
[68] 楠山春樹, "呂氏春秋＜中＞", 新編漢文選思想・歴史シリーズ, 明治書院 (1997).
[69] 李玉, " " 鬼屎 " 考", 吉林農業大学学報, **24**, 2, pp. 1–4 (2002).
[70] L. Villarreal, "Algunas especies de myxomycetes no registradas del estado de veracruz", 18, pp. 153–164 (1983).
[71] 萩原博光, 山本幸憲, 伊沢正名, "日本変形菌類図鑑", 平凡社 (1995).
[72] 杉山純多編, "菌類・細菌・ウイルスの多様性と系統", バイオディバーシティ・シリーズ 4, 裳華房 (2005).
[73] S. L. Stephenson and H. Stempen, "Myxomycetes; a handbook of slime molds", Timber Press (1994).
[74] W. D. Gray and C. J. Alexopoulos, "Biology of the Myxomycetes", The Ronald Press, 1st ed. (1968).
[75] H. C. Aldrich and J. W. Daniel Eds., "Cell biology of *Physarum* and *Didymium*; organisms, nucleus, and cell cycle" (1982).
[76] O. Brefeld, "Dictyostelium mucoroides; ein neuer organismus aus der verwandtshaft der myxomyceten", Abhandlungen der Senckenbergischen Naturforschenden Gesellschaft, **7**, pp. 85–107 (1869).
[77] H. A. de Bary, "Morphologie und Physiologie der Pilze, Flechten und Myxomyceten"

(1866).
[78] E. Haeckel, “Generelle Morphologie der Organismen”, Georg Reimer (1866).
[79] R. H. Whittaker, “New concepts of kingdoms of organisms”, Science, **163**, 3863, pp. 150–160 (1969).
[80] L. Margulis and K. V. Schwartz, “Five kingdoms; an illustrated guide to the phyla of life on earth”, W. H. Freeman (1982).
[81] S. M. Adl, A. G. Simpson, M. A. Farmer, R. A. Andersen, O. R. Anderson, J. R. Barta, S. S. Bowser, G. Brugerolle, R. A. Fensome, S. Fredericq, et al., “The new higher level classification of eukaryotes with emphasis on the taxonomy of protists”, Journal of Eukaryotic Microbiology, **52**, 5, pp. 399–451 (2005).
[82] S. M. Adl, A. G. Simpson, C. E. Lane, J. Lukeš, D. Bass, S. S. Bowser, M. W. Brown, F. Burki, M. Dunthorn, V. Hampl, et al., “The revised classification of eukaryotes”, Journal of Eukaryotic Microbiology, **59**, 5, pp. 429–514 (2012).
[83] M. Poulain, M. Meyer and J. Bozonnet, “Les Myxomycètes”, Fédération mycologique et botanique Dauphiné-Savoie (2011).
[84] M. Carlile and J. Dee, “Plasmodial fusion and lethal interaction between strains in a myxomycete.”, Nature, **215**, 5103, p. 832 (1967).
[85] 神谷宣郎, “粘菌変形体の運動特性”, 蛋白質核酸酵素, **28**, 5, pp. p424–437 (1983).
[86] F. Bramstedt, “Dressurversuche mit *Paramecium caudatum* und *Stylonychia mytilus*”, Zeitschrift für vergleichende Physiologie, **22**, 4, pp. 490–516 (1935).
[87] L. M. Day and M. Bentley, “A note on learning in paramecium.”, Journal of Animal Behavior, **1**, 1, p. 67 (1911).
[88] I. Kunita, S. Kuroda, K. Ohki and T. Nakagaki, “Attempts to retreat from a dead-ended long capillary by backward swimming in paramecium”, Frontiers in Microbiology, **5**, p. 270 (2014).
[89] I. Kunita, T. Yamaguchi, A. Tero, M. Akiyama, S. Kuroda and T. Nakagaki, “A ciliate memorizes the geometry of a swimming arena”, Journal of The Royal Society Interface, **13**, 118 (2016).
[90] 中垣俊之, “粘菌 その驚くべき知性”, PHP サイエンス・ワールド新書, PHP 研究所 (2010).
[91] A. Tero, K. Yumiki, R. Kobayashi, T. Saigusa and T. Nakagaki, “Flow-network adaptation in physarum amoebae”, Theory in Biosciences, **127**, 2, pp. 89–94 (2008).
[92] I. Kunita, K. Yoshihara, A. Tero, K. Ito, C. F. Lee, M. D. Fricker and T. Nakagaki, “Adaptive path-finding and transport network formation by the amoeba-like organism physarum”, Natural Computing and Beyond, Springer, pp. 14–29 (2013).
[93] A. Adamatzky, “Route 20, autobahn 7, and slime mold: approximating the longest roads in usa and germany with slime mold on 3-d terrains”, Cybernetics, IEEE Transactions on, **44**, 1, pp. 126–136 (2014).
[94] A. Adamatzky and J. Jones, “Road planning with slime mould: If physarum built motorways it would route m6/m74 through newcastle”, International Journal of Bifurcation and Chaos, **20**, 10, pp. 3065–3084 (2010).
[95] T. Saigusa, A. Tero, T. Nakagaki and Y. Kuramoto, “Amoebae anticipate periodic events”, Phys. Rev. Lett., **100**, p. 018101 (2008).
[96] S. Takagi, Y. Nishiura, T. Nakagaki, T. Ueda and K.-I. Ueda, “Indecisive behavior of amoeba crossing an environmental barrier”, Topological Aspects of Critical Systems and Networks: Proceedings of the International SymposiumWorld Scientific

Publishing, pp. 86–93 (2007).
[97] M. Aono, Y. Hirata, M. Hara and K. Aihara, "Amoeba-based chaotic neurocomputing: Combinatorial optimization by coupled biological oscillators", New Generation Computing, **27**, 2, pp. 129–157 (2009).
[98] J. B. Lamarck, "Zoological philosophy", Macmillan and Co., Limited, translated by Hugh Elliot (1914).
[99] Y.-P. Gunji, T. Shirakawa, T. Niizato and T. Haruna, "Minimal model of a cell connecting amoebic motion and adaptive transport networks", Journal of theoretical biology, **253**, 4, pp. 659–667 (2008).
[100] J. Jones, "The emergence and dynamical evolution of complex transport networks from simple low-level behaviours.", Int. Journ. of Unconventional Computing, **6**, 2, pp. 125–144 (2010).
[101] Y. Liu, Z. Zhang, C. Gao, Y. Wu and T. Qian, "A physarum network evolution model based on ibtm", Advances in Swarm Intelligence, Springer, pp. 19–26 (2013).
[102] Y. Liu, C. Gao, M. Liang, L. Tao and Z. Zhang, "A physarum-inspired vacant-particle model with shrinkage for transport network design", International Conference in Swarm IntelligenceSpringer, pp. 74–81 (2015).
[103] 恒藤敏彦, "弾性体と流体", 物理入門コース 8, 岩波書店 (1983).
[104] N. Kamiya, "Protoplasmic Streaming", Vol. 8 of Protoplasmatologia Handbuch der Protoplasmaforschung, Springer Vienna (1959).
[105] A. V. Bykov, A. V. Priezzhev, J. Lauri and R. Myllylä, "Doppler oct imaging of cytoplasm shuttle flow in physarum polycephalum", Journal of biophotonics, **2**, 8-9, pp. 540–547 (2009).
[106] 服藤憲司, "グラフ理論による回路解析", 森北出版 (2014).
[107] K. Thulasiraman and M. N. S. Swamy, "Graphs: Theory and Algorithms", Wiley-Interscience (1992).
[108] F. L. Howard, "Laboratory cultivation of myxomycete plasmodia", American Journal of Botany, pp. 624–628 (1931).
[109] W. G. Camp, "A method of cultivating myxomycete plasmodia", Bulletin of the Torrey Botanical Club, pp. 205–210 (1936).
[110] A. L. Cohen, "Nutrition of the myxomycetes. i. pure culture and two-membered culture of myxomycete plasmodia", Botanical Gazette, pp. 243–275 (1939).
[111] A. Cohen, "Nutrition of the myxomycetes. ii. relations between plasmodia, bacteria, and substrate in two-membered culture", Botanical Gazette, pp. 205–224 (1941).
[112] J. Daniel and H. Rusch, "The pure culture of physarum polycephalum on a partially defined soluble medium", Journal of general microbiology, **25**, 1, pp. 47–59 (1961).
[113] W. Baumgarten and M. J. Hauser, "Detection, extraction, and analysis of the vein network", Journal of Computational Interdisciplinary Sciences, **1**, 3, pp. 241–249 (2010).
[114] W. Baumgarten and M. J. Hauser, "Computational algorithms for extraction and analysis of two-dimensional transportation networks", J. Comput. Interdiscip. Sci, **3**, pp. 107–16 (2012).
[115] B. Obara, V. Grau and M. D. Fricker, "A bioimage informatics approach to automatically extract complex fungal networks", Bioinformatics, **28**, 18, pp. 2374–2381 (2012).
[116] N. Suwa, T. Niwa, H. Fukasawa and Y. Sasaki, "Estimation of intravascular blood

pressure gradient by mathematical analysis of arterial casts", The Tohoku journal of experimental medicine, **79**, 2, pp. 168–198 (1963).

[117] H. Passing and W. Bablok, "A new biometrical procedure for testing the equality of measurements from two different analytical methods. application of linear regression procedures for method comparison studies in clinical chemistry, part i", Clinical Chemistry and Laboratory Medicine, **21**, 11, pp. 709–720 (1983).

[118] H. Passing and W. Bablok, "Comparison of several regression procedures for method comparison studies and determination of sample sizes application of linear regression procedures for method comparison studies in clinical chemistry, part ii", Clinical Chemistry and Laboratory Medicine, **22**, 6, pp. 431–445 (1984).

[119] E. Manuilova, A. Schuetzenmeister and F. Model, "mcr: Method comparison regression", `https://cran.r-project.org/package=mcr`.

[120] M. Fricker, M. Tlalka, D. Bebber, S. Tagaki, S. Watkinson and P. Darrah, "Fourier-based spatial mapping of oscillatory phenomena in fungi", Fungal Genetics and Biology, **44**, 11, pp. 1077 – 1084 (2007).

[121] R. D. Guy, T. Nakagaki and G. B. Wright, "Flow-induced channel formation in the cytoplasm of motile cells", Phys. Rev. E, **84**, p. 016310 (2011).

[122] D. Helbing, I. Farkas and T. Vicsek, "Simulating dynamical features of escape panic", Nature, **407**, 6803, pp. 487–490 (2000).

[123] A. Kirchner, K. Nishinari and A. Schadschneider, "Friction effects and clogging in a cellular automaton model for pedestrian dynamics", Phys. Rev. E, **67**, p. 056122 (2003).

[124] A. Takamatsu and T. Fujii, "Construction of a living coupled oscillator system of plasmodial slime mold by a microfabricated structure", Sensors Update, **10**, 1, pp. 33–46 (2002).

[125] A. Takamatsu, T. Fujii and I. Endo, "Control of interaction strength in a network of the true slime mold by a microfabricated structure", Biosystems, **55**, 13, pp. 33 – 38 (2000).

[126] W. Stockem and K. Brix, "Analysis of microfilament organization and contractile activities in physarum", Vol. 149 of International Review of Cytology, Academic Press, pp. 145 – 215 (1994).

[127] I. Kunita, K. Sato, Y. Tanaka, Y. Takikawa, H. Orihara and T. Nakagaki, "Shear banding in an f-actin solution", Phys. Rev. Lett., **109**, p. 248303 (2012).

[128] A. Kamiya and T. Togawa, "Adaptive regulation of wall shear stress to flow change in the canine carotid artery", American Journal of Physiology - Heart and Circulatory Physiology, **239**, 1, pp. H14–H21 (1980).

[129] J. Haskovec, P. Markowich and B. Perthame, "Mathematical analysis of a pde system for biological network formation", Communications in Partial Differential Equations, **40**, 5, pp. 918–956 (2015).

[130] J. Haskovec, P. Markowich, B. Perthame and M. Schlottbom, "Notes on a pde system for biological network formation", Nonlinear Analysis: Theory, Methods & Applications, **138**, pp. 127 – 155 (2016).

[131] J. Gräwer, C. D. Modes, M. O. Magnasco and E. Katifori, "Structural self-assembly and avalanchelike dynamics in locally adaptive networks", Phys. Rev. E, **92**, p. 012801 (2015).

Appendix

MATLAB code of the simulation

Below we show the source code of the simulation. Typing command `evacCR('result.mat')` with black and white images in the current directory named `shapeC.gif`, `shapeR1.gif`, `shapeR2.gif`, `shapeR3.gif`, `shapeR4.gif`, `shapeR5.gif`, and `shapeR5.gif` will generate simulated result file `result.mat`. The result is saved in cell arrays for each shapes, and each cell has dimensions of μ and time, possibly with another dimension of index of vertex or edge. For example, radius of edge with index of 3 at $t = 1$ of the simulation with $\mu = 4/1$ in shape R5 is referred by `R{find(ismember(shapes, 'R5'))}(3, find(times==1), 1)`.

```
function evacCR(savename)

shapes = {'C', 'R1', 'R2', 'R3', 'R4', 'R5', 'A'}; % Name of shape
evacp = [703 1222; 536 1885; 546 1603; ...
644 1126; 873 888; 1126 626; 561 714]; % Coordinate of exit
times = [0:0.001:0.1, 0.11:0.01:1, 1.1:0.1:500]; % times
app = 500; % arena per random mesh point
qpp = 0.1; % quantity of divergence
RND = 20160606; % random seed
four_mu = 1:5; % 4/mu
r0 = 0.1; % initial radius

% function handles for time evolution
dr = cell(length(four_mu));
fnames = cell(length(four_mu)); % function names
for i = 1:length(four_mu)
dr{i} = @(rx, qx) (qx.^(4./four_mu(i))-rx.^4)./(4.*rx.^3);
fnames{i} = strcat('mu4_', strrep(num2str(four_mu(i)),'.','_'));
end

% initialization of cells
R = cell(length(shapes),1); % radius
Q = R; % flow rate
V = R; % pressure
```

```
D = R; % conductivity to exit
En = R; % total friction energy
Vol = R; % total volume
pos = R; % positions of vertices
EG = R; % connectivity information of edges

tic
clock0 = round(clock());
parfor i = 1:length(shapes)
rng(RND);
mask_BW = (imread(['shape' shapes{i} '.gif'])>0); % read arena image
[pos{i}, EG{i}] = rMesh(mask_BW, evacp(i,:), app); % generate random mesh

VN = size(pos{i},1); % number of vertices
EN = size(EG{i},1); % number of edges

V0 = find((pos{i}(:,1)==evacp(i,1))&(pos{i}(:,2)==evacp(i,2)));
% exit vertex
V1 = setdiff(1:VN, V0); % other vertices
vI = [V1' V1']; % information of divergence
vI(:,2) = qpp; % same divergence
vI = [vI; V0 zeros(length(V0),1)]; % 0 for exit, see findD

% initialization of contents of cells
R{i} = r0.*ones(EN, length(times), length(fnames)); % initial radii
Q{i} = ones(EN, length(times), length(fnames));
V{i} = ones(VN, length(times), length(fnames));
D{i} = ones(VN, length(times), length(fnames));
En{i} = ones(length(times), length(fnames));
Vol{i} = ones(length(times), length(fnames));

% initial quantities
len = sqrt(sum((pos{i}(EG{i}(:,1),:)-pos{i}(EG{i}(:,2),:)).^2, 2));
% length of edge
EG{i}(:,3) = len./R{i}(:,1,1).^4; % resistance of edge

[Vinit, Dinit] = findD(EG{i}, vI);
% find initial pressure and conductivity to exit
Qinit = abs(Vinit(EG{i}(:,1))-Vinit(EG{i}(:,2)))./EG{i}(:,3);
% apply values for all initial state of mu
Q{i}(:, 1, :) = repmat(Qinit, 1, 1, size(Q{i},3));
V{i}(:, 1, :) = repmat(Vinit, 1, 1, size(V{i},3));
D{i}(:, 1, :) = repmat(Dinit, 1, 1, size(D{i},3));
En{i}(1, :) = ...
sum(abs(Vinit(EG{i}(:,1))-Vinit(EG{i}(:,2))).^2./EG{i}(:,3));
Vol{i}(1, :) = sum(len.*pi.*R{i}(:,1,1).^2);
```

```
count = 0;
countmax = length(fnames)*length(times);
for j = 1:length(fnames)
for k = 2:length(times)
[R{i}(:,k,j), Q{i}(:,k,j), V{i}(:,k,j), D{i}(:,k,j)] = ...
CRstep(pos{i}, EG{i}, R{i}(:,k-1,j), vI, dr{j}, times(k)-times(k-1));
En{i}(k,j) = ...
sum(Q{i}(:,k,j).*abs(V{i}(EG{i}(:,1),k,j)-V{i}(EG{i}(:,2),k,j)));
Vol{i}(k, j) = sum(len.*pi.*R{i}(:,k,j).^2);

etime(round(clock()),clock0)
            count = count + 1;
disp([shapes{i} ': ' fnames{j} ': ' num2str(count/countmax*100)])
end
end
end
toc

save(savename);
toc

end


function [R, Q, V, D] = CRstep(pos, EG, R0, vI, dr, dt)
%CRstep One step of time evolution of current-reinforcement
% [R, Q, V, D] = CRstep(pos, EG, R0, vI, dr, dt)
%
% pos: n rows and 2 columns, where n is the number of vertices
% EG: m rows and 2 columns, where m is the number of edges
% R0: initial radius of the edges, m rows and 1 columns
% vI: divergences of each vertex, n rows and 2 columns see also findD
% dr: a function handle or an anonymous function,
% by which radii are developed as r = r + dr(r,q).*dt
% dt: time step
%
% The outputs are quantities of the next time:
% R: radii of the edges
% Q: flow rate of the edges
% V: pressure of the vertices
% D: conductance of each vertex to the exits
%
l = sqrt( sum( ( pos(EG(:,1),:) - pos(EG(:,2),:) ).^2, 2) );
R = R0;
EG(:,3) = l./R.^4;
```

```
[V, D] = findD(EG, vI);
Q = abs(V(EG(:,1))-V(EG(:,2)))./EG(:,3);

R = R + dr(R,Q).*dt;
EG(:,3) = 1./R.^4;
[V, D] = findD(EG, vI);
Q = abs(V(EG(:,1))-V(EG(:,2)))./EG(:,3);
end


function [V, D] = findD( EG, vI )
%findD Find voltages and conductivity to ground for current sources
% [V, D] = findD( EG, vI )
%
% EG: n rows and 3 columns, where 1st and 2nd columns indicate edge,
% and 3rd columns resistance of the edge.
% The resistance must be greater than 0, allowing Inf.
% vI: current sources and grounds
% 1st column is indices of vertex.
% 2nd column is the quantity of current source.
% If the 2nd column is 0,
% corresponding vertex is regarded as grounded.
%
% Outputs
% V: Voltages of each vertex
% D: Coductivity to ground at each vertex
%
v = unique([EG(:,1); EG(:,2)]); % list of vertices
VN = max(v); % number of vertices
vI = sortrows(vI);
V0 = [setdiff(1:VN,v)'; vI(vI(:,2)==0,1)]; % grounds
V1 = vI(vI(:,2)~=0,1); % not grounded
egN = size(EG,1); % number of edges

% Conductivity matrix
ConMat = zeros(VN);
pmMat = [1 -1; -1 1];
for i=1:egN
ConMat(EG(i,1:2),EG(i,1:2)) = ...
ConMat(EG(i,1:2),EG(i,1:2)) + pmMat/EG(i,3);
end
% erase rows and columns regarding grounded vertices
ConMat(V0,:)=[];
ConMat(:,V0)=[];
ConMat = sparse(ConMat);
```

```
% find conductivity
Vmat = inv(ConMat);
D = zeros(VN,1);
D(setdiff(1:VN,V0)) = diag(Vmat);
D(V0) = 0;
D = 1./D;

% find voltage
b = zeros(VN,1);
b(V1) = vI(vI(:,2)~=0,2);
b(V0) = [];
V = zeros(VN,1);
V(setdiff(1:VN,V0)) = sum(Vmat*diag(b),2);

end


function [pos, EG] = rMesh(mask, pmust, app)
%rMesh Make rondom mesh
% [pos EG] = rMesh(mask, pmust, app)
% mask: matrix of which elements are 0 or 1
% pmust: points which must be included
% app: area per point
% pos: positions of points
% EG: list of edges

r = sqrt(3*app/pi);

% make random vertices in whole image
ranN = ceil(length(mask(:))/app); % number of vertices
pos = unique([randi(size(mask,2),ranN,1) ...
randi(size(mask,1),ranN,1)],'rows'); % random positions
pos(ismember(pos,pmust,'rows'),:) = [];
% exclude points of the same position to pmust
pos = [pmust; pos];
posi = 1:size(pos,1); % position index

% triangulation in whole image
DT = delaunay(pos(:,1:2)); % Delaunay triangulation
EG = unique(sort([DT(:,1:2); DT(:,2:3); DT(:,[3 1])],2),'rows'); % edges

% crop the network by the position of vertices
inBW = mask(sub2ind(size(mask),pos(:,2),pos(:,1)))==1; % in mask
EG( (~inBW(EG(:,1)))|(~inBW(EG(:,2))), :) = [];
% exclude edges with vertices not in
posi(~inBW) = []; % exclude vertices not in (from posi)
```

```
% relabel position index of EG
for i=1:length(pos)
EG(EG(:)==i) = find(posi==i);
end
pos(~inBW,:) = []; % exclude vertices from pos

% crop by edges out of mask
maskY = imdilate(mask, strel('disk',round(r/4)));
% enlarged mask including cropped network
l = sqrt( sum( ( pos(EG(:,1),1:2) - pos(EG(:,2),1:2) ).^2, 2) );
% length of edge
inBW = ones(size(EG,1),1); % in mask
for i=1:size(EG,1)
p0 = pos(EG(i,1),1:2);
pp = pos(EG(i,2),1:2) - pos(EG(i,1),1:2);
% check the edge is in maskY for each pixel
for j=1:round(l(i))
pj = p0 + j*pp/l(i);
inBW(i) = inBW(i)&maskY(round(pj(2)),round(pj(1)));
end
end
EG = EG(inBW==1,:); % exclude edges not in

end
```